TFBP-TR-289
for U.S. Nuclear Regulatory Commission

REACTIVITY INITIATED ACCIDENT TEST SERIES
RIA SCOPING TEST
QUICK LOOK REPORT

Z.R. MARTINSON R.S. SEMKEN
T. INABE R.H. SMITH
T.F. COOK A.D. APPELHANS

September 1978

EG&G Idaho, Inc.

IDAHO NATIONAL ENGINEERING LABORATORY

DEPARTMENT OF ENERGY

IDAHO OPERATIONS OFFICE UNDER CONTRACT EY-76-C-07-1570

TFBP-TR-289
for U.S. Nuclear Regulatory Commission

REACTIVITY INITIATED ACCIDENT TEST SERIES
RIA SCOPING TEST
QUICK LOOK REPORT

Z.R. MARTINSON R.S. SEMKEN
T. INABE R.H. SMITH
T.F. COOK A.D. APPELHANS

September 1978

EG&G Idaho, Inc.

IDAHO NATIONAL ENGINEERING LABORATORY

DEPARTMENT OF ENERGY

IDAHO OPERATIONS OFFICE UNDER CONTRACT EY-76-C-07-1570

TFBP-TR-289
September 1978

REACTIVITY INITIATED ACCIDENT TEST SERIES

RIA SCOPING TEST

QUICK LOOK REPORT

Z. R. Martinson
R. S. Semken
T. Inabe
R. H. Smith
T. F. Cook
A. D. Appelhans

A. S. Mehner, Supervisor
PCM, RIA, and IE Tests Section

R. K. McCardell, Manager
Experiment Specification and Analysis Branch

P. E. MacDonald, Manager
Light Water Reactor Fuel Research Division

CONTENTS

FIGURES

TABLES

SUMMARY

The Reactivity Initiated Accident Scoping Test (RIA-ST) was successfully completed August 30, 1978. The test was introductory to the RIA Series 1 tests and was designed to investigate and resolve several anticipated problem areas prior to performance of the first test of the series, Test RIA 1-1. The RIA Scoping Test, as performed, consisted of four separate single-rod experiment phases. The first three phases were performed with shrouded fuel rods of 5.8 wt.% enrichment. They were subjected to power bursts resulting in total fuel surface energies ranging from 205 to 261 cal/g at the axial peak elevation. The fourth phase consisted of a 20 wt.% enriched, shrouded fuel rod which was subjected to a power burst that deposited a total radially averaged energy of 527 cal/g.

The primary objectives of the Scoping Test were defined as follows:

(1) Determine the applicability of extrapolating low-power steady state calorimetric measurements and self-powered neutron detector (SPND) output to determine fuel rod energy depositions during a power burst.

(2) Determine the energy deposition failure threshold for unirradiated fuel rods at BWR hot-startup coolant conditions.

(3) Determine the magnitudes of possible pressure pulses resulting from rod failure.

(4) Determine the sensitivity of the test instrumentation to high transient radiation exposures.

In general, the energy deposition values for the Scoping Test derived from the SPND output were 25% higher than those obtained from the core ion chamber data . Determining which values are correct will

require radiochemical analysis of the fuel rods which will take several months. At present, it appears that the SPND derived energies are in error because of excellent agreement between the calculated and measured power calibration results and the agreement between the predicted failure threshold and that seen using the core ion chamber derived energies.

Meeting the second objective was accomplished during the first three test phases by subjecting the fuel rods to energy depositions which bracketed the failure threshold. The failure threshold in terms of total pellet surface energy at the axial flux peak was found to be between 218 cal/g where no rod failure occurred and 256 cal/g where rod failure did occur. The experiment predictions indicated that the failure threshold would be 262 cal/g at the pellet surface.

Only the fourth experiment phase (527 cal/g) resulted in a pressure pulse upon rod failure. The best indication of source pressure was the reading from a 69 MPa EG&G pressure transducer at the flow shroud inlet. This pressure transducer indicated a pressure pulse upon rod failure of 28.2 MPa with a rise time of 1.6 ms. The source pressure was attenuated considerably outside the shroud region as indicated by pressure transducers in the upper plenum of the in-pile tube and in the flow bypass region. The maximum pressure indicated outside the flow shroud was 2.1 MPa.

In general, instrumentation sensitivity to radiation was minimal. The most significant instrumentation problem during the power bursts was a false flowrate indication by the flow turbines. This problem is being examined. The Kaman and Bell & Howell pressure transducers showed the least sensitivity to radiation of the pressure measurement devices. The EG&G transducers were most sensitive. The locked linear variable differential transformer (LVDT) gave no indication of radiation sensitivity as its response during the burst was a straight line. The strain gages were very sensitive to radiation,

indicating a strain increase of 70% with the second burst of RIA-ST-1. The Type S thermocouple did not exhibit significant radiation sensitivity.

In addition, the RIA Scoping Test has provided data on the consequences of fuel rod failure during a RIA event at BWR hot startup conditions. Posttest examination of the fuel rods from the first two phases of the test revealed large quantities of UO_2 fuel missing from the cladding. Fuel rod failures for energy depositions near the failure threshold in previous closed capsule tests without forced coolant flow resulted in only a slight amount of fuel loss.

1. INTRODUCTION

The Reactivity Initiated Accident Scoping Test (RIA-ST), performed in the EG&G operated Power Burst Facility (PBF), was completed on August 30, 1978. The Scoping Test was the introductory test to the five planned PBF/RIA tests of Series 1[a]. The objectives of the RIA Series 1 tests are to determine the thresholds, modes, and consequences of fuel failure under RIA conditions as functions of energy deposition, irradiation history, and fuel rod design. Each test will be performed with coolant conditions typical of commercial boiling water reactors (BWR) during hot-startup. With the completion of the RIA Scoping Test, four previously identified questions which relate to the successful performance of the RIA Series 1 tests have been addressed. The four questions which were to be answered by the RIA Scoping Test are: (1) Can low-power steady state calorimetric measurements and self-powered neutron detector output be extrapolated to determine fuel rod energy depositions during a power burst? (2) What is the energy deposition failure threshold for unirradiated fuel rods with BWR hot startup coolant conditions? (3) What is the magnitude of possible pressure pulses that can result from fuel rod failure in a water filled system? and (4) What is the sensitivity of the test instrumentation to high transient radiation exposures?

The RIA Scoping Test was originally comprised of five separate single-rod experiment phases designated as RIA-ST-1, RIA-ST-2, RIA-ST-3, RIA-ST-4, and RIA-ST-5. The RIA-ST-5 experiment was cancelled, and therefore will not be discussed in this report. Section 2

---

[a] The Series 1 tests consist of Tests RIA 1-1, RIA 1-2, RIA 1-3, and RIA 1-6 (shrouded four-rod tests) and RIA 1-4 (a sixteen-rod cluster test).

provides a brief description of the design of the four RIA Scoping Test experiments performed. Section 3 outlines the test conduct, providing results of the power calibrations and the magnitudes of the power bursts. Test results are presented in Section 4 in terms of the test objectives and where applicable are compared to the experimental predictions. Section 5 contains six photographs illustrating the posttest condition of the rods from RIA-ST-2 and RIA-ST-3. These two rods were subjected to energy depositions which bracket the failure threshold deposition. In Section 6, a brief discussion of the fission products detection subsequent to the test rod failures is presented, and finally, Section 7 provides conclusions.

2. TEST DESIGN

The RIA Scoping Test as performed was comprised of four separate, single-rod experiment phases. The fuel rod for each phase was positioned in a separate flow shroud in the center of the PBF in-pile tube (IPT). The non-instrumented high-pressure spool pieces were installed in the loop piping. This section describes the design of the fuel rods, test assembly, and instrumentation associated with each experiment.

2.1 Test Train

The four fuel rods used in the RIA Scoping Test experiment phases were designated as 800-1, 800-2, 800-3, and 800-4, respectively. The nominal design characteristics of these rods are given in Table I. The fuel rods were fabricated from unirradiated cladding and fresh fuel pellets. The fuel pellets for Rods 800-1, 800-2, and 800-3 were ground down to fit in the available pressurized water reactor (PWR) cladding.

Individual zircaloy-4 flow shrouds, having a nominal inner diameter of 16.3 mm and an outer diameter of 22.6 mm, surrounded Rods 800-1, 800-2, and 800-3. A zircaloy-4 flow shroud, having a nominal inner diameter of 19.3 mm and an outer diameter of 25.4 mm, surrounded Rod 800-4. Fuel particle catch screens were installed at the inlet and outlet of the flow shroud for Rod 800-4.

The PBF single rod test train assembly was used for the RIA Scoping Test. In this test assembly, the fuel rod is held rigidly at the top, with the rod free to expand axially downward.

2.2 Instrumentation

The RIA Scoping Test instrumentation was intended for pressure pulse measurement, calorimetric measurement of the test rod power, and evaluation of instrumentation to be used in future RIA tests. There

TABLE I

RIA SCOPING TEST FUEL ROD DESIGN CHARACTERISTICS

Characteristic	Rods 800-1, 2, 3	Rod 800-4
Fuel		
Material	UO_2	UO_2
Pellet OD (mm)	8.23	9.3
Pellet length (mm)	15.2	15.49
Pellet enrichment (wt. %)	5.8	20
Density(% TD)	94	93
Fuel stack length (m)	0.914	0.914
End configuration	Dished	Dished
Burnup	0	0
Cladding		
Material	Zr-4	Zr-4
Tube OD (mm)	9.70	10.73
Tube wall thickness (mm)	0.64	0.61
Fuel Rod		
Overall length (m)	1.0	1.0
Filler gas	Helium	Helium
Initial gas pressure (MPa)	0.103	3.79

was no instrumentation installed on the test fuel rods. Table II summarizes the instrumentation used for the RIA Scoping Test including information as to location, range, and response time. Figure 1 provides a schematic representation of the test train in the IPT flow tube showing the approximate locations of some of the test train instrumentation.

The test assembly instrumentation consisted of the following:

(1) Three coolant pressure transducers; two located above the flow shroud outlet, and one connected to the flow shroud to measure normal system pressure and transient pressure pulses. All these pressure transducers were operable through the four experiments.

(2) Two turbine flowmeters, mounted in series at the inlet of the flow shroud, to measure the shroud coolant flow. Both turbine flowmeters failed in the course of the test. One replacement was necessary.

(3) Four Chromel-Alumel (Type K) thermocouples; two mounted at the shroud inlet and two at the outlet, to measure the fuel rod coolant temperature at inlet and outlet. One inlet and one outlet thermocouple failed during the course of the test.

(4) Two differential copper-constantan (Type T) thermocouples mounted on the test train to measure the fuel rod coolant temperature rise. One of these was broken during a rod changeout.

(5) Three cobalt SPNDs located in one vertical column 30 degrees clockwise from the reactor north position at 0.229, 0.457, and 0.686 m above the bottom of the test fuel rod.

(6) One flux wire, mounted on the outer surface of the flow shroud (reactor north orientation), for each phase of the

TABLE II

TEST TRAIN INSTRUMENTATION FOR RIA-ST

Measurement	Instrument	Instrument Location	Instrument Range	Response Time (s)
Coolant pressure	Pressure transducer	Upper plenum	0 to 69 MPa	3×10^{-5}
Coolant pressure	Pressure transducer	Upper plenum	0 to 17 MPa	3×10^{-5}
Coolant pressure	Pressure transducer	Connected to shroud	0 to 69 MPa	3×10^{-5}
Coolant flow	Turbine flow meters (2)	Inlet of flow shroud	63 to 820 cm^3/sec	N/A
Coolant inlet temperature	Thermocouples (2)	Inlet of flow shroud	300 to 600 K	N/A
Coolant outlet temperature	Thermocouples (2)	Outlet of flow shroud	300 to 600 K	N/A
Coolant differential temperature	Thermocouple pairs (2)	Inlet and outlet of flow shroud	0 to 20 K	N/A
Relative neutron flux	Cobalt SPNDs (3)	1 vertical column with detectors at 0.229, 0.457, and 0.686 m from bottom of fuel stack	N/A	0.002
Neutron flux (IPT)	0.5% cobalt wire for Rods 1, 4, and 5 100% cobalt wire for Rods 2 and 3 [a]	Outer surface of flow shroud (reactor North orientation)	N/A	N/A
Neutron flux (core)	100% cobalt wire	PBF core periphery	N/A	N/A
Cladding elongation	LVDT	Bottom of fuel rod	-5 to 20 mm	0.003
Radiation sensitivity	Pressure transducer (4)	Upper plenum	0 to 17 MPa (3) 0 to 69 MPa	0.002
Radiation sensitivity	Pressure transducer (1)	Flow bypass region	0 to 17 MPa	0.002
Radiation sensitivity	LVDT	Lower plenum	0 ± 12.7 mm	0.003
IPT head temperature	Type K thermocouple	IPT head	30 to 600 K	N/A
Shroud strain	Strain gauge (2)	Flow shroud of Rod 1 only	-1% to +1%	Not known

[a] Rod 1 refers to Rod 800-1, Rod 2 refers to Rod 800-2, etc.

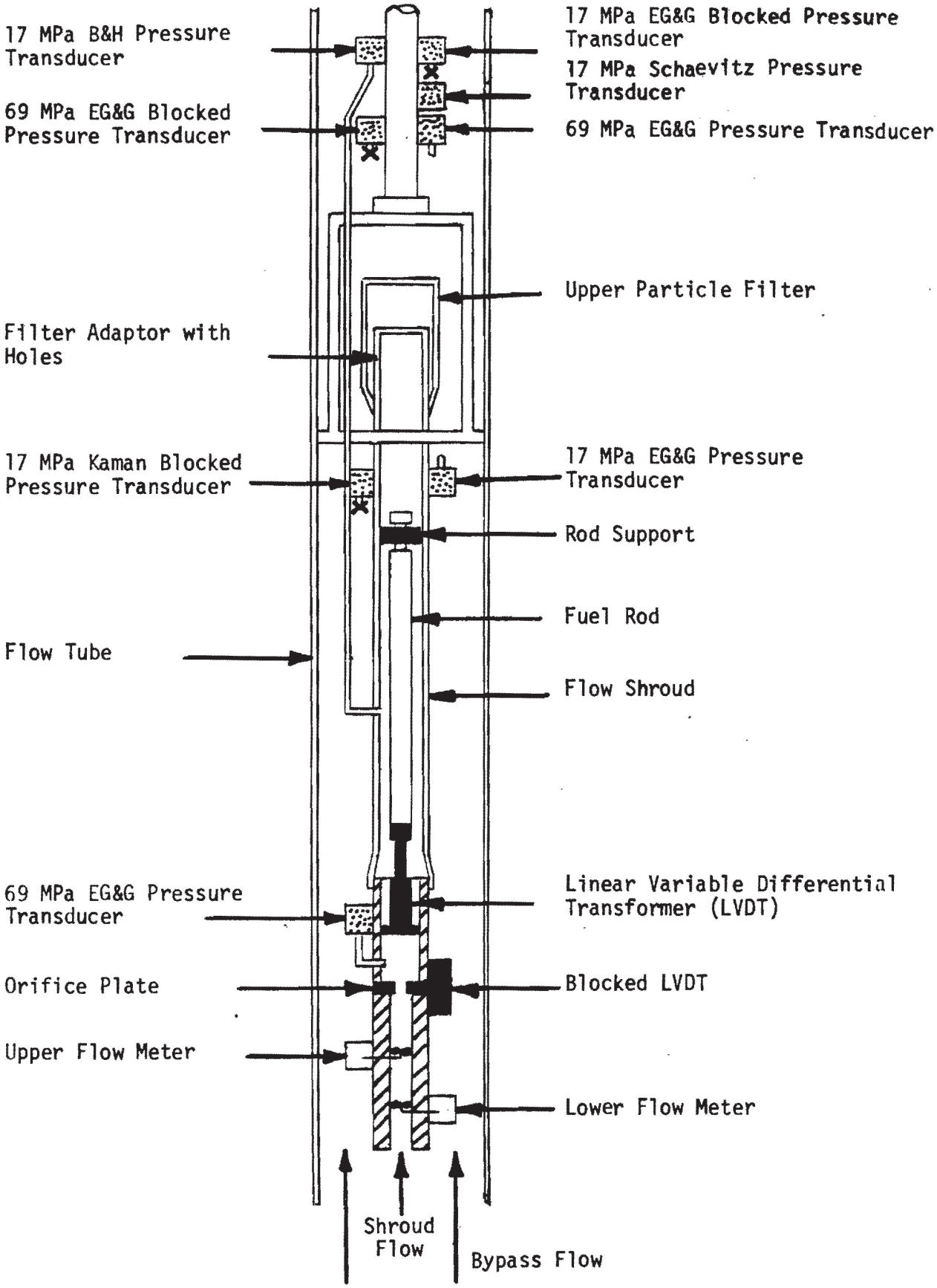

Fig. 1 Schematic representation of RIA Scoping Test train showing approximate instrument locations.

test (0.51% Co-Al wire for Rods 800-1 and 800-4, and 100% cobalt wire for Rods 800-2 and 800-3).

(7) One Kaman pressure transducer, and two EG&G DC excited strain post type pressure transducers, located in the flow bypass region for radiation sensitivity evaluation. The pressure transducers were sealed to eliminate instrument response due to coolant pressure changes. The pressure transducers were backfilled with helium to a cold pressure of 2.07 MPa.

(8) One Bell and Howell pressure transducer and one Schaevitz pressure transducer located above the flow shroud outlet for instrument evaluation. The Schaevitz transducer failed prior to running the first experiment. The Bell and Howell pressure transducer was connected via a tube welded to the flow shroud at the axial power peak elevation for RIA-ST-4.

(9) An LVDT mounted at the bottom of the fuel rod to measure changes in the axial length of the rod. This LVDT failed prior to RIA-ST-1 and its housing was removed after RIA-ST-2 was completed in order to improve the pressure pulse measurements for RIA-ST-4.

(10) An LVDT with the core locked in position, located below the fuel rod for radiation sensitivity evaluation.

(11) One Type S thermocouple, located on the flow shroud, for radiation sensitivity evaluation. This thermocouple was only connected for RIA-ST-1.

(12) Two Type K thermocouples to measure the IPT head temperature.

(13) Two strain gages, located on the flow shroud, for radiation sensitivity evaluation. These were connected only during RIA-ST-1.

Plant instrument data recorded along with the test train instrument data were the following:

(1) NMS-3 ion chamber

(2) PPS-1, PPS-2, PPS-3, PPS-4 ion chambers

(3) TR-1, TR-2 ion chambers

(4) EV-1, EV-2 ion chambers

(5) In-pile tube system pressure

(6) In-pile tube ΔP

(7) Loop flow rate

(8) Loop fission product detection system

(9) Core fuel rod LVDTs (2)

(10) Reactor vessel strain gages (2)

(11) Loop pressure transducers (9)

In addition, a 100% cobalt flux wire was installed in the reflector region of the core. A new cobalt flux wire was installed during each scheduled reactor shutdown. A closed-circuit television camera was positioned to view the Heise loop pressure gage and the image was displayed on a television monitor at the PBF control room.

The test assembly and plant instrument data were recorded on the PBF Data Acquisition and Reduction System (PBF/DARS), Surveillance System (SS), and Experiment and Analysis System (E&A).

3. TEST CONDUCT

The RIA Scoping Test as performed was comprised of the four separate, single-rod test phases designated as RIA-ST-1, RIA-ST-2, RIA-ST-3, and RIA-ST-4. Each of the single-rod experiments was proceeded by a non-nuclear heat up and interspersed with a number of instrument status checks as specified in the RIA Scoping Test Experiment Operating Specification[1]. The purpose of these instrument verification procedures was to identify failed or out-of-range instrumentation so that corrective action could be initiated before proceeding with the test and to insure that instrumentation critical to the experiment was operable. Table III summarizes the as performed activities associated with RIA-ST-1 through RIA-ST-4. Several revisions were made to the RIA-ST Experiment Operating Specification during the test. The revisions are described in Document Revision Request (DRR) forms.

The nuclear operational phases of the test are reviewed below.

3.1 Power Calibration

The objective of the power calibration portion of RIA-ST-1 and RIA-ST-4 was to intercalibrate the thermal-hydraulically determined fuel rod power with reactor neutron detecting chambers and the SPNDs mounted on the test train. The on-line power calibrations were accomplished by measuring the coolant pressure, coolant inlet temperature, coolant temperature rise, and experiment flow. An axial peak-to-average neutron flux ratio of 1.36 was used. The nominal coolant conditions for the power calibration phases were 538 K inlet temperature, 6.45 MPa IPT pressure, and 760 cm^3/s experiment flow. The results of the power calibration portion of RIA-ST-1 and RIA-ST-4 are summarized in Tables IV and V and Figures 2 through 5. Power calibration conversion ratios for the test fuel rods of 2.2 and 5.2 kW/m per MW of PBF core power were measured for RIA-ST-1 and RIA-ST-4, respectively. Reactor physics calculations had predicted a power calibration conversion ratio of 2.15 kW/m per MW of PBF core power for the 5.8% enriched rods used in RIA-ST-1.

TABLE III

RIA SCOPING TEST CONDUCT

RIA-ST-1	RIA-ST-2	RIA-ST-3	RIA-ST-4
Heatup	Heatup	Heatup	Heatup
Power Calibration	Power Burst[a] (240 cal/g)	Power Burst[a] (204 cal/g)	Power Calibration
Shutdown	Cooldown	Cooldown	Shutdown
Core Flux Wire Change			Core Flux Wire Change
Power Calibration			Power Burst[a] (527 cal/g)
Shutdown			
Core Flux Wire Change			
Conditioning			
Shutdown			
Core Flux Wire Removal			
Control Rod Worth Check			
Trial Transient			
Shutdown			
Core Flux Wire Installation			
Power Burst (192 cal/g)[a]			
Core Flux Wire Change			
Power Burst (244 cal/g)[a]			
Cooldown			

[a]Fuel rod energy refers to the total radially averaged value at the axial power peak location including 15.3 cal/g for ambient temperature of 538 K.

TABLE IV

SUMMARY OF RIA-ST-1 POWER CALIBRATION DATA

Reactor Power (MW)	Test Rod Peak Power (kW/m)	Axial Midplane SPND Current (nA)	System Coolant Pressure (MPa)	Coolant Flow Rate (cm^3/s)	Coolant Inlet Temperature (K)	Temperature Rise Across Experiment (K)
5.5	14.6	48.4	6.36	754.0	539.7	3.3
8.6	22.3	70.8	6.42	769.5	538.2	4.9
11.2	28.6	108.4	6.43	759.1	540.3	6.3
11.2	28.3	106.7	6.42	768.1	538.4	6.2
14.1	35.0	136.0	6.43	752.0	538.1	7.8
14.3	35.4	138.8	6.43	750.4	537.8	7.9
16.9	41.2	162.0	6.42	758.7	537.7	9.1
16.9	40.9	163.3	6.43	756.0	537.9	9.0
19.8	46.9	187.0	6.42	760.5	538.6	10.3
21.8	51.1	201.3	6.41	767.9	538.3	11.1
19.8	47.2	183.8	6.43	752.7	538.4	10.4
16.9	40.9	163.7	6.42	763.0	536.7	9.0
14.3	34.7	138.7	6.42	766.8	537.4	7.6
11.4	28.5	111.2	6.42	764.7	536.3	6.3
8.9	22.5	85.7	6.43	755.0	536.6	5.0
5.7	15.4	56.5	6.42	766.0	536.0	3.4
2.8	7.9	28.3	6.43	749.6	535.0	1.8

TABLE V

SUMMARY OF RIA-ST-4 POWER CALIBRATION DATA

Reactor Power (MW)	Test Rod Peak Power (kW/m)	Axial Midplane SPND Current (nA)	System Coolant Pressure (MPa)	Coolant Flow Rate (cm^3/s)	Coolant Inlet Temperature (K)	Temperature Rise Across Experiment (K)
2.6	14.7	28.1	6.42	7771.0	537.1	3.2
3.8	22.0	43.2	6.42	777.0	537.7	4.7
5.0	28.6	56.6	6.42	773.6	537.7	6.2
6.5	36.2	71.6	6.42	776.8	538.9	7.8
7.3	40.4	81.6	6.41	782.1	536.4	8.6
8.9	48.4	97.7	6.42	786.6	539.2	10.5
8.8	48.1	96.4	6.42	768.4	538.5	10.4
9.6	51 6	104.1	6.42	766.6	538.4	11.2
8.7	47.0	94.7	6.42	763.7	538.4	10.2
7.0	38.8	78.1	6.42	764.9	539.1	8.5
5.8	33.0	66.1	6.42	766.6	538.8	7.2
4.7	26.6	52.9	6.42	765.7	538.2	5.8
3.4	20.1	39.4	6.42	767.5	538.7	4.4
2.0	12.1	22.4	6.42	768.2	538.4	2.7

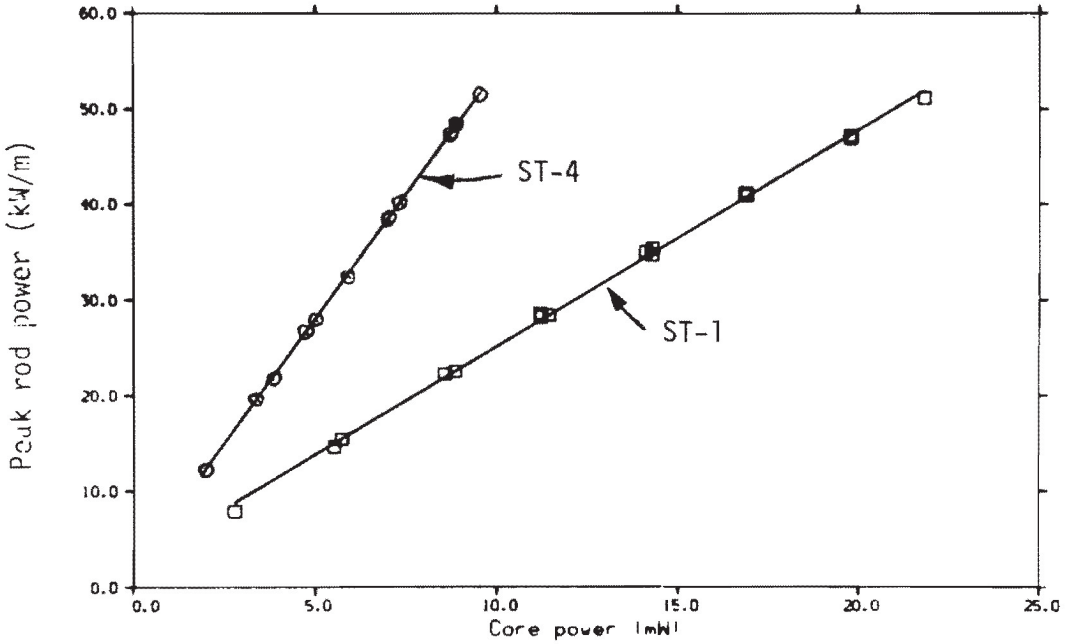

Fig.2 Peak rod power as a function of core power (RIA-ST-1, ST-4)

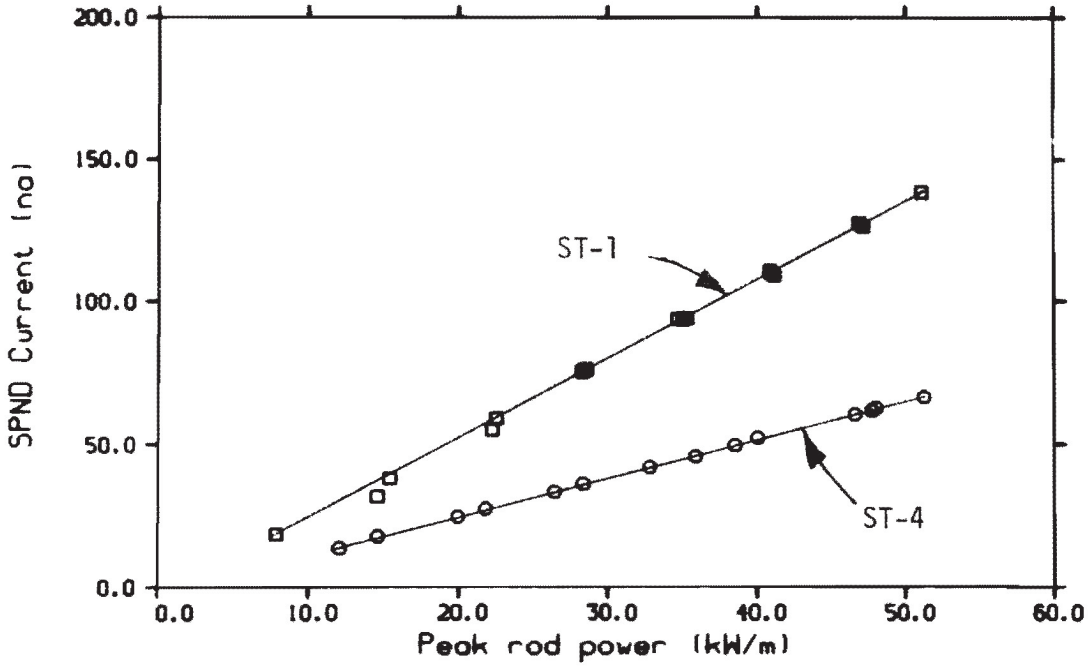

Fig.3 SPND(.686) Current vs peak rod power (RIA ST-1,ST-4)

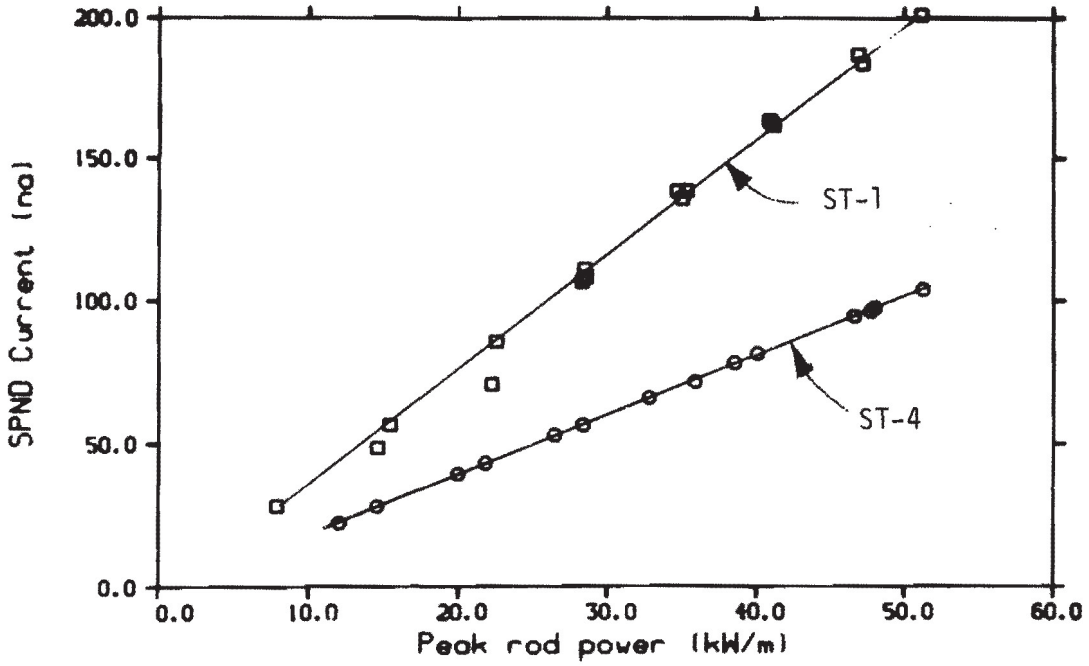

Fig. 4 SPND(.457) Current vs peak rod power (RIA ST-1,ST-4)

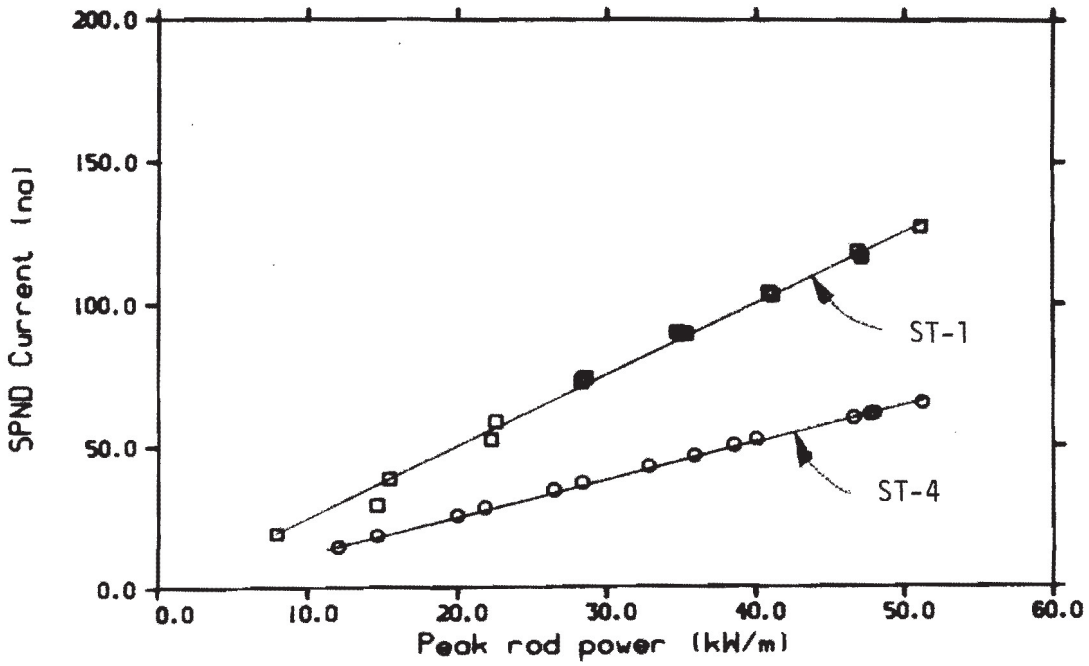

Fig. 5 SPND(.229) Current vs peak rod power (RIA ST-1,ST-4)

3.2 Fuel Rod Conditioning

The objectives of the conditioning portion of RIA-ST-1 were to buildup the fission product inventory of the fuel rod to assure cladding failure indication by the fission product detection system during the transient testing and to cause fuel cracking and fuel relocation. The conditioning phase consisted of 4 power cycles. During each cycle the fuel rod peak power was increased slowly to 52 kW/m, held constant for 5 minutes, and then slowly reduced to 3 kW/m and held constant for 5 minutes. The maximum power ramp rate was 3 kW/m per minute. The nominal operating conditions were 538 K inlet temperature, 6.45 MPa IPT pressure, and 760 cm^3/s experiment flow. The reactor was shut down after the fuel rod conditioning was completed to replace the core flux wire.

3.3 Control Rod Worth and Transient Checkout

Control rod reactivity worth checks and a trial reactor transient were performed after the power calibration and conditioning. The control rod reactivity worth checks were intended to intercalibrate the control rods and transient rods for reactivity worths of 0.75, 1.5, and 1.75 dollars. A reactivity meter was used to measure the reactivity worth of the transient rods during transient rod insertion. The control rods were intercalibrated with the transient rods by determining the control rod position required for reactor criticality with the transient rods inserted in the core the required amount. Actual power bursts were not performed for the 1.5 and 1.75 dollar reactivity measurements. A trial power burst (1.7 s period - 13 MW peak power) was performed for the 0.75 dollar reactivity measurement to verify the control rod and transient rod worth measurements indicated by the reactivity meter. The loop operating conditions in this phase were 538 K inlet temperature, 6.45 MPa coolant pressure, and 760 cm^3/s shroud flow. Results indicate that the accuracy of the reactivity meter measurements ($\pm$0.10 dollars) was not adequate to permit determination of the actual control rod positions for performing a pre-selected power burst.

3.4 Power Burst Testing

A total of five power bursts, excluding the previously discussed trial transient, were run in the course of the RIA Scoping Test. Reactor primary coolant conditions for each were nominaly 15,000 gpm, 295 K at the inlet, and atmospheric pressure. The test loop conditions for each of the power bursts were nominally 85 cm^3/s, 538 K at the flow shroud inlet, and 6.45 MPa. Each transient was initiated by the following sequence of events.

(1) The reactor was made critical at about 100 W for determination of the low power critical position of the control rods.

(2) From this position the control rods were withdrawn an amount required to establish a reactor transient period of approximately 10 s. The reactor power was allowed to increase until the "chamber operable" light indicated that the plant protective chambers were functioning properly. Immediately upon reaching this level, the control rods were inserted an amount required to make the reactor subcritical causing the power to rapidly decrease.

(3) The transient rods were then drawn into the core to a position representative of the reactivity insertion required for the power burst.

(4) The control rods were then withdrawn to make the reactor critical at a low power level. The reactivity inserted by the withdrawal of the control rods and the worth of the transient rods was compared to assure the increment of control rod withdrawal determined for the power burst was not grossly in error.

(5) The control rods were adjusted, if required, to the increment of withdrawal determined for the desired reactivity insertion.

(6) The transient rods were then fully inserted into the core.

(7) The power burst was initiated manually by firing the transient rods, rapidly removing poison from the core. The reactor was set to scram at 0.15 seconds after transient initiation or at 9,900 MW for the first burst and at 0.09 seconds or at 16,500 MW for the subsequent four power bursts.

Results of the power burst testing are discussed in further detail in Section 3.5.

3.5 Power Bursts

The power burst testing consisted of two power bursts during RIA-ST-1 and one power burst for each of RIA-ST-2, RIA-ST-3, and RIA-ST-4. The test rod energy deposition data for the five power bursts are summarized in Table VI. Fuel rod failure occurred in all of the phases except RIA-ST-3. A brief discussion of the power burst testing is given below.

3.5.1 RIA-ST-1 Power Bursts. A total pellet surface energy of 205 cal/g UO_2 at the axial flux peak was deposited during the first power burst. No indication of fuel rod failure was observed. As shown in Figure 6, both of the 69 MPa EG&G pressure transducers located at the ends of the flow shroud indicated a series of small amplitude pressure disturbances probably caused by the sudden steam formation and water expulsion from the flow shroud following the power burst.

As illustrated by Figure 7, the shroud inlet flow turbines indicated a rapid flow increase at about the time of peak power. This

TABLE VI

RIA SCOPING TEST SUMMARY

TRANSIENT NUMBER	REACTOR PERIOD (ms)	TOTAL RADIALLY AVERAGED ENERGY[a] (CAL/G UO_2)	TOTAL PELLET SURFACE ENERGY[a] (CAL/G UO_2)	ROD FAILURE
RIA-ST-1 PB-1	5.7	192	205	NO
RIA-ST-1 PB-2	4.4	244	261	YES
RIA-ST-2	4.6	239	256	YES
RIA-ST-3	5.2	204	218	NO
RIA-ST-4	3.85	527	849	YES

[a] Total energy includes 15.3 cal/g UO_2 for ambient temperature of 538 K. Fuel rod energy values are based on the core ionization chamber data. Fuel rod energy values based on SPND output are about 25% higher. This discrepancy is discussed in Section 4.1.

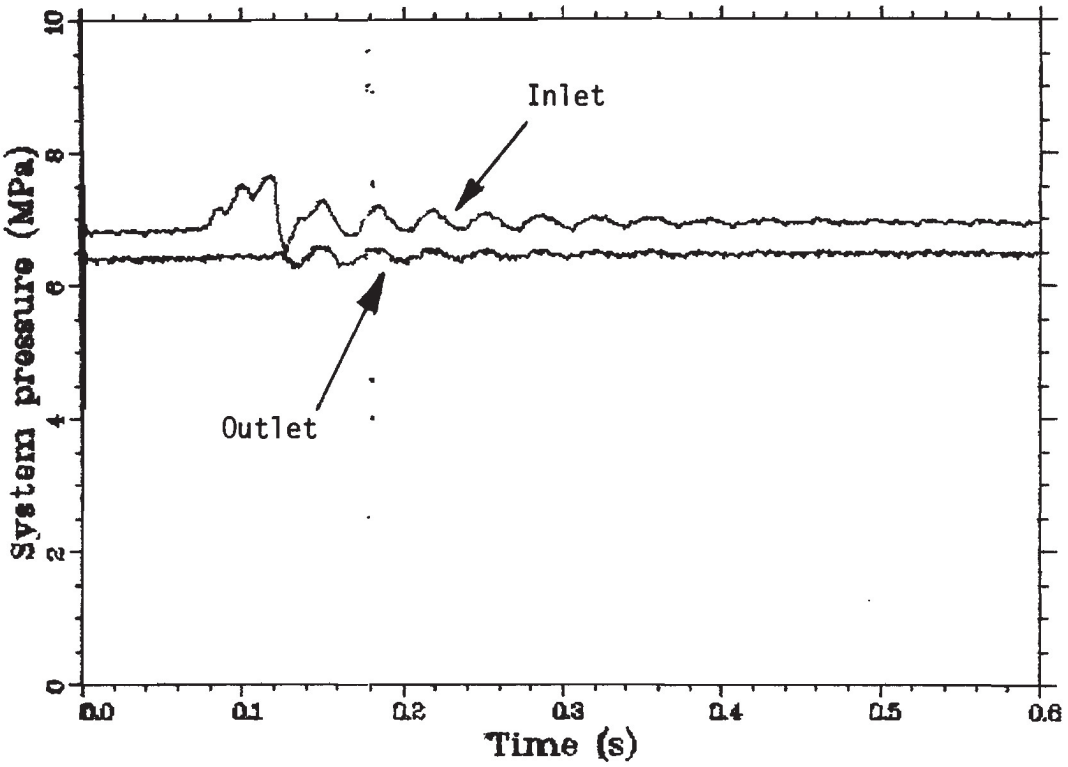

Fig.6 Coolant pressure vs. time at the flow shroud inlet and outlet during the first power burst of RIA-ST-1 as indicated by the 69 MPa EG&G pressure transducers.

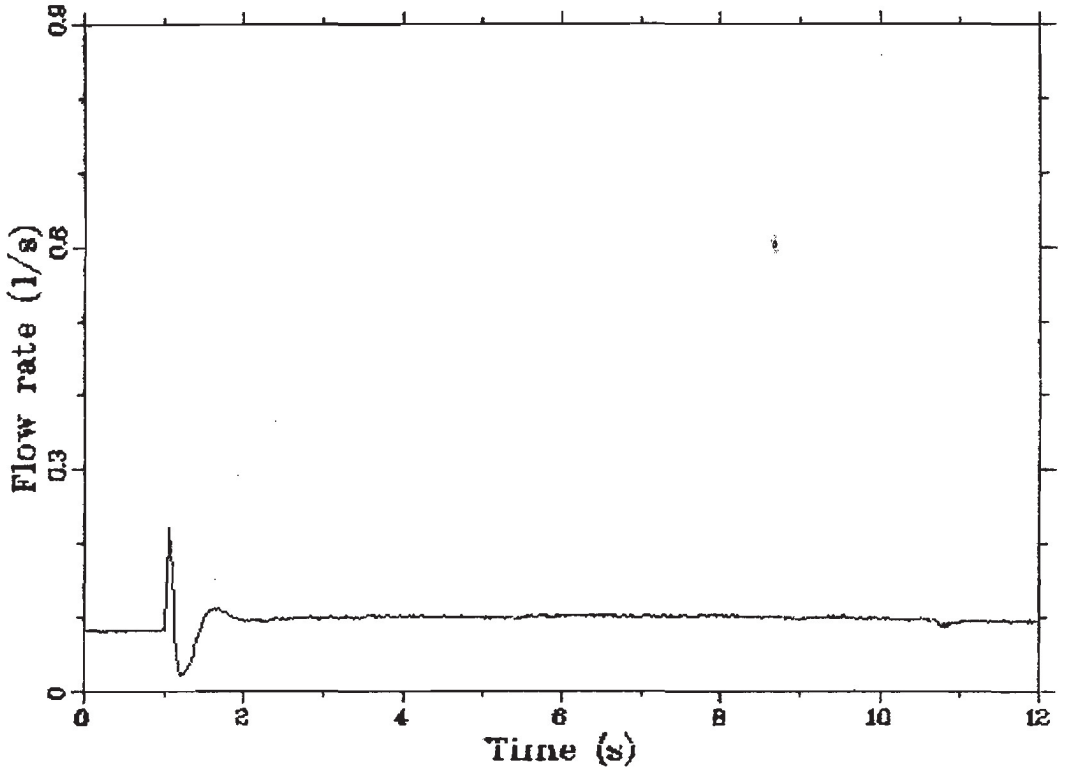

Fig.7 Shroud coolant flowrate at the inlet during the first power burst of RIA-ST-1.

indicated flow increase, observed in all five power bursts, is believed to be incorrect and due to radiation sensitivity of the flow turbine pick-up coil or signal conditioning electronics. More will be said about this problem in Section 4.4.

The second power burst of RIA-ST-1, performed on the same rod used in the first burst, deposited a total pellet surface energy of 261 cal/g UO_2 at the axial flux peak. The first indication of fuel rod failure was from a plant radiation monitor located near the test loop piping in the basement of the reactor building. Approximately six minutes following the power burst, rod failure was indicated by a sharp increase in the radiation field. Rod failure was also indicated about 1.5 minutes later by the fission product detection system. None of the pressure transducers or other test train instruments indicated the time of rod failure. The exact time of fuel rod failure is uncertain due to the long time necessary for coolant to flow from the fuel rod to the radiation monitor locations.

3.5.2 RIA-ST-2 Power Burst. The RIA-ST-2 fuel rod was exposed to a single power burst with no significant steady state operation. The pellet surface energy of 256 cal/g UO_2 deposited during the single power burst resulted in fuel rod failure. The loop monitor indicated failure about 7 minutes and the fission product detection system about 7.5 minutes after the power burst. None of the test train instrumentation indicated fuel rod failure.

3.5.3 RIA-ST-3 Power Burst. The RIA-ST-3 fuel rod was subjected to a single power burst which deposited a pellet surface energy of 218 cal/g UO_2 at the axial flux peak. Neither the loop monitor or the fission product detector indicated fuel rod failure.

3.5.4 RIA-ST-4 Power Burst. After the power calibration was completed for RIA-ST-4, the fuel rod was subjected to a single power burst which deposited 527 cal/g UO_2 radially averaged at the axial flux peak or 849 cal/g at the fuel pellet surface. As expected, this large energy deposition resulted in immediate fuel rod failure. A

large pressure pulse was recorded by the lower 69 MPa EG&G pressure transducer connected to the lower end of the flow shroud. The Bell and Howell pressure transducer, connected via small diameter tubing to the flow shroud at the axial flux peak elevation, indicated a pressure pulse which exceeded the 17 MPa rating of the transducer. The time of the pressure increase was about 4 ms after the time of peak power. The fuel rod total energy, radially averaged at axial flux peak, was 280 cal/g UO_2 at the time of rod failure. This corresponds to a fuel surface energy of 447 cal/g. Further discussion of the pressure pulse detected during RIA-ST-4 can be found in Section 4.3.

The fission product detection system indicated rod failure about 3.25 minutes after the power burst. The loop radiation monitor indicated rod failure within two minutes after the power burst. Data from the fission product detection system are discussed in detail in Section 6.

4. TEST RESULTS

Test results presented herein correspond to one of the four questions (Section 1) which made up the objective of the RIA Scoping Test. Where applicable, the results of pretest predictions are included to compare with the test data.

4.1 Applicability of Calorimetric Measurements to Power Burst Testing

The first objective of the RIA Scoping Test was to evaluate the applicability of extrapolating low-power calorimetric measurements to determine fuel rod energy depositions during a power burst. Radiochemical analysis to directly measure the power burst fuel rod energy deposition in the RIA Series 1 program tests will not be possible due to extensive operation for preconditioning the fuel rods before the power burst.

Relating the calorimetric power calibration results of the RIA Scoping Test to the response of each of four core neutron detecting chambers was used to measure the fuel rod energy deposition during each power burst.

Reactor physics calculations were made of the test rod and PBF core rod values of energy per fission during steady state and transient operation. These calculated values were used to convert test rod power per core power during steady state operation to cal/g UO_2 per core energy release during a power burst. The output of the core neutron detecting chambers during each power burst was integrated to yield the total core energy release. The core energy release was multiplied by the test rod energy deposition per core energy release ratio in terms of cal/g UO_2 per MJ.

A similar procedure was also used to measure fuel rod energy deposition by relating the calorimetric power calibration results to the three SPNDs. The output of each SPND was integrated during a power burst. The integrated detector output was multiplied by the

cal/g UO_2 per SPND output current·seconds which was determined from the steady state power calibration data. The fuel rod energy values determined from the four core neutron chambers and the three SPNDs are given in Table VII. Data from the EV-2 core ionization chamber were not included in the preliminary estimates of fuel rod energy for each power burst since this ionization chamber consistently indicated higher powers and core energies than the other three ionization chambers. It appears that the chamber intercalibration constants were incorrect for EV-2.

Note in Table VII that the fuel rod energy values as determined from the three SPNDs are about 25% higher than those obtained from the core ionization chambers. The cause of this discrepancy is not known, but some possible reasons are:

(1) The axial power profile in the IPT for a power burst may be different than the profile during steady state operation. The 0.229 m and the 0.686 m SPNDs indicate fuel rod energies about 15% higher than the 0.457 m SPND. Scan measurements of the cobalt flux wires attached to the outer surface of the flow shrouds have not been completed to date, but will provide profile information prior to the RIA Series 1 tests. Data from the SPNDs indicate only slight differences in the steady state and transient power profiles.

(2) The time response of the SPNDs and associated electronics may not be adequate to follow a rapid power burst. A comparison of the PBF core power during RIA-ST-3 as derived from the 0.229 m SPND and the TR-1 core ionization chamber is shown in Figure 8. The power-time curve shapes for the two detectors are similar, but the SPND indicates higher power during the entire power burst. The similarity of the two curves implies that the SPND and associated electronics time response characteristics are not the problem.

TABLE VII

SUMMARY OF FUEL ROD ENERGY DATA[a]

Test Designation	Fuel Rod Energy From Core Chamber TR-1 (Cal/g UO_2)	Fuel Rod Energy From Core Chamber TR-2 (Cal/g UO_2)	Fuel Rod Energy From Core Chamber EV-1 (Cal/g UO_2)	Fuel Rod Energy From Core Chamber EV-2 (Cal/g UO_2)	Fuel Rod Energy From 0.229 m SPND (Cal/g UO_2)	Fuel Rod Energy From 0.457 m SPND (Cal/g UO_2)	Fuel Rod Energy From 0.686 m SPND (Cal/g UO_2)	Fuel Rod Energy From TR-1, TR-2, and EV-1 Core Chamber (Cal/g UO_2)	Fuel Rod Energy From Three SPNDs (Cal/g UO_2)	Difference in Fuel Rod Energy Values for Core Chambers and SPNDs (Percent)
RIA-ST-1 Power Burst-1	195	191	188	211	266	212	251	192	243	21
RIA-ST-2 Power Burst-2	245	242	244	270	343	294	338	244	325	25
RIA-ST-2	241	235	240	259	348	291	330	230	323	26
RIA-ST-3	202	205	204	208	287	262	276	204	275	26
RIA-ST-4	523	Data Problem	531	571	617	Data Problem	611	527	614	14

[a] All values refer to radially-average total fuel rod energy at axial flux peak.

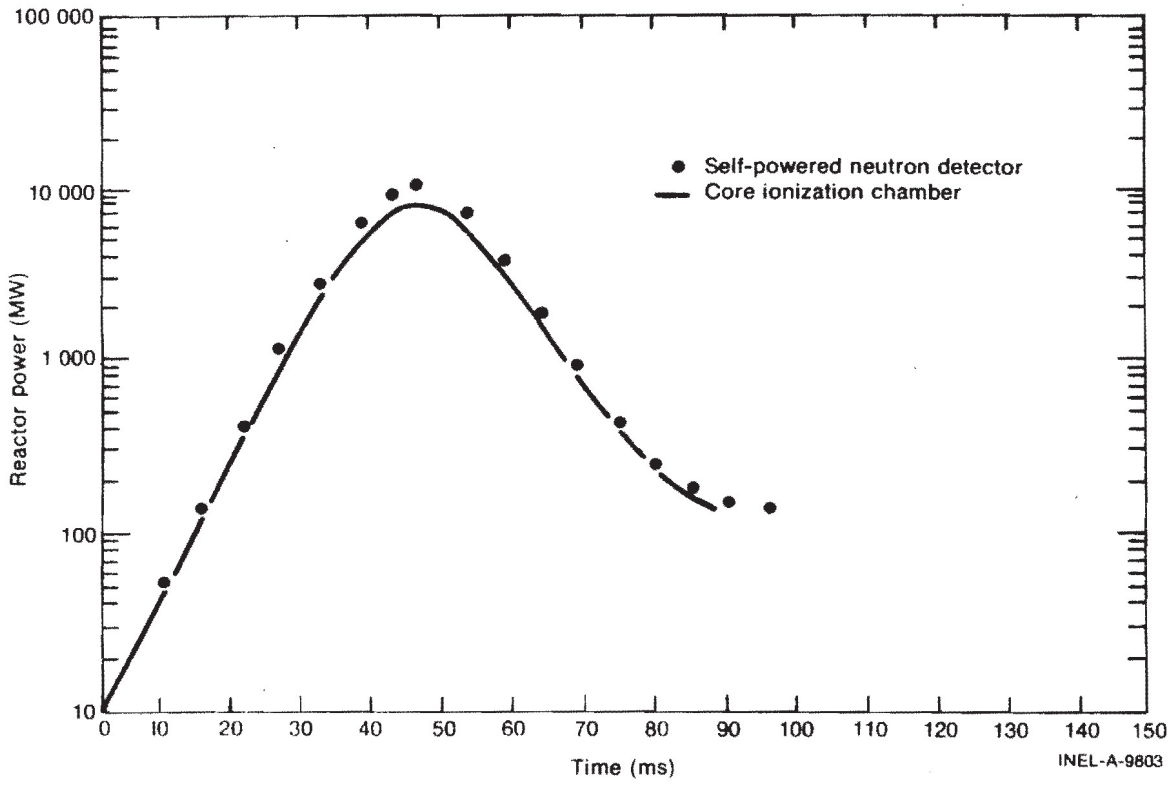

Fig. 8 Comparison of PBF core power during RIA-ST-3 as derived from 0.229 SPND and TR-1 core ionization chamber.

(3) The steady state calibration of the SPNDs in terms of SPND current output per test rod power may not be correct for power burst testing. The SPND data was multiplied by the ratio of test rod energy per fission during a power burst to test rod energy per fission during steady state operation, namely

$$\frac{172.2 \text{ MeV/fission}}{183.8 \text{ MeV/fission}} .$$

The preliminary fuel rod energy values given in this report were determined from the core ionization chambers. These values were chosen in preference to the SPND derived data because the core chamber data was in excellent agreement with reactor physics calculations. Reactor physics pretest calculations performed by the EG&G Reactor Physics Engineering Branch using a one-dimensional neutron-transport code predicted a test rod power per core power for RIA-ST-1 of 2.15 kW/m/MW versus 2.2 measured. A reactor physics calculation was not made for the RIA-ST-4 fuel rod since previous PCM Test Series power calibration results were available. In addition, if the SPND derived fuel rod energy data is used, then the fuel rod in RIA-ST-3 received a radially averaged energy of 275 cal/g UO_2 or 296 cal/g UO_2 at the pellet surface and yet did not fail. Fuel rod failure is predicted to occur at a pellet surface energy of 262 cal/g UO_2.

The actual fuel rod energy depositions for the RIA Scoping Test power bursts will not be determined for several months when the radiochemical analysis is completed. The accuracy of the procedures will be checked by radiochemical analysis of fuel samples from the fuel rods tested in RIA-ST-2 and RIA-ST-3. The irradiation history for these two rods was limited to single power bursts, so that the radiochemical analysis will represent only the transient energy deposition.

4.2 Failure Threshold

Another objective of the RIA Scoping Test was determining the energy deposition failure threshold for the 5.8 wt% enriched fuel rods under commercial Boiling Water Reactor hot startup conditions. The RIA Scoping Test Experiment Predictions Report[2] identified the threshold as 262 cal/g deposited at the fuel pellet surface. From the results of the RIA-ST-1, RIA-ST-2, and RIA-ST-3 experiments (refer to Table VI) the failure threshold can be assumed to be between 218 cal/g where the fuel rod did not fail (RIA-ST-3) and 256 cal/g where the rod did fail (RIA-ST-2), using the energy depositions determined from the output of the core ionization chambers. The prediction is slightly above this range but in general agreement.

Presented in Section 5 are photographs taken of the fuel rods of RIA-ST-2 and RIA-ST-3, respectively. The severity of failure of the RIA-ST-2 rod and the appearance of the RIA-ST-3 rod indicates that the failure threshold is probably close to midway between the energy depositions of the RIA-ST-2 and RIA-ST-3 experiments. For Test RIA 1-1, therefore, it can be assumed, based on the photographs and supported by the pretest prediction, that a fuel surface energy of approximately 240 cal/g will be sufficient to induce rod failure.

4.3 Pressure Pulse Generation

The primary reason for the investigation into pressure pulse generation produced by RIA-induced rod failure is concern for the integrity of the PBF in-pile tube (IPT). Prior to running the Series 1 tests, an evaluation of maximum possible pressure pulses was made. As will be seen in this section, the source pressure which resulted from the rod failure in RIA-ST-4 was significant, however the pressures at the wall of the IPT were quite low.

Rod failures occurred in the second burst of RIA-ST-1, in RIA-ST-2, and in RIA-ST-4. Figure 9 illustrates coolant pressure with respect to time at the shroud inlet and in the upper plenum of the IPT

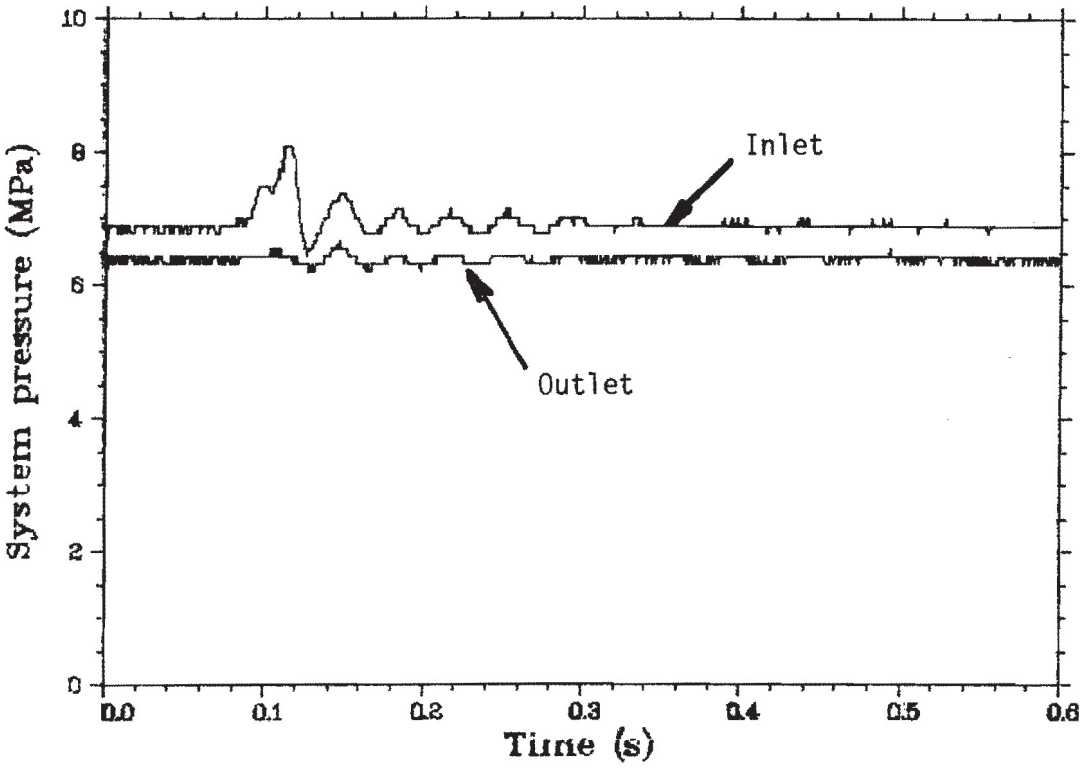

Fig. 9 Coolant pressure vs. time at flow shroud inlet and outlet during the second power burst of RIA-ST-1 as indicated by the 69 MPa EG&G pressure transducers.

subsequent to the second power burst of RIA-ST-1. The figure shows the same pressure oscillations seen in Figure 6 of Section 3.5.1. As pointed out in Section 3.5.1, the small amplitude pressure disturbances were probably caused by the sudden steam formation and water expulsion from the flow shroud due to the rapid heat transfer from the fuel rod following the power burst. It appears that at low energy depositions, there is no significant pressure pulse generation. This assumption is supported by the experiment predictions.

The rod failure of RIA-ST-4, however, was immediate and violent. For this test there were four pressure transducers capable of detecting the resulting pressure pulse as it was attenuated from the source to the walls of the in-pile tube. Figures 10 through 13 show the pressure history following the RIA-ST-4 power burst for each transducer. Referring to Figure 1 to determine approximate transducer location, it can be seen that the 17 MPa EG&G pressure transducer (pressure trace in Figure 10) is outside the flow shroud near the top of the test rod. This transducer has the least direct view of the source pressure. Figure 10 indicates that a maximum pressure increase in the bypass region of 1.8 MPa with a 4 ms rise time resulted from the source pressure.

The upper 69 MPa EG&G pressure transducer is attached to the hanger rod above the shroud outlet and beyond the upper particle filter. Figure 11, depicting the pressure history indicated by the upper 69 MPa transducer, shows a pressure increase of 2.1 MPa with a 3 ms rise time.

Figure 12 shows the pressure trace from the 17 MPa Bell and Howell pressure transducer. This device was connected via a small diameter tube to the axial power peak location in the inside of the flow shroud. The Bell & Howell pressure transducer was most directly in view of the source pressure and would have given the best representation of it. However as shown by Figure 12, the pressure transducer saturated as a result of the source pressure pulse and did not provide the magnitude of the pressure pulse or a rise time. The transducer

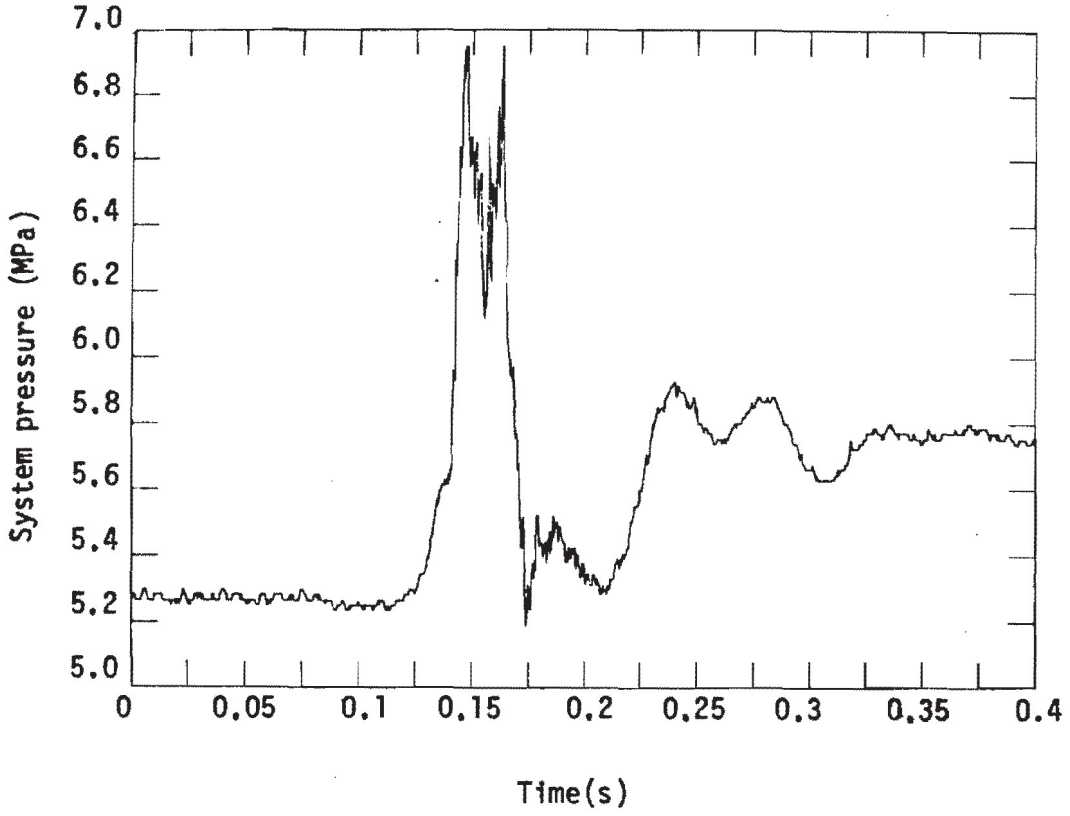

Fig. 10 Response of the 17 MPa EG&G pressure transducer during the power burst of RIS-ST-4.

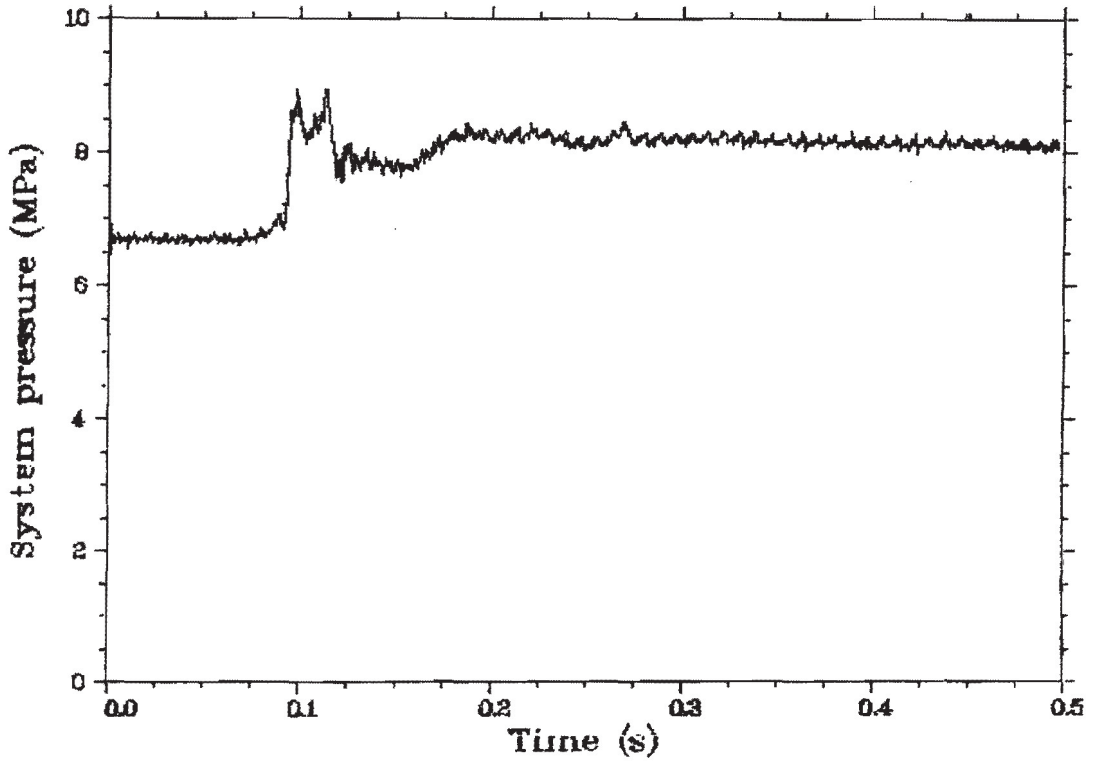

Fig.11 Response of the upper 69 MPa EG&G pressure transducer during the power burst of RIA-ST-1.

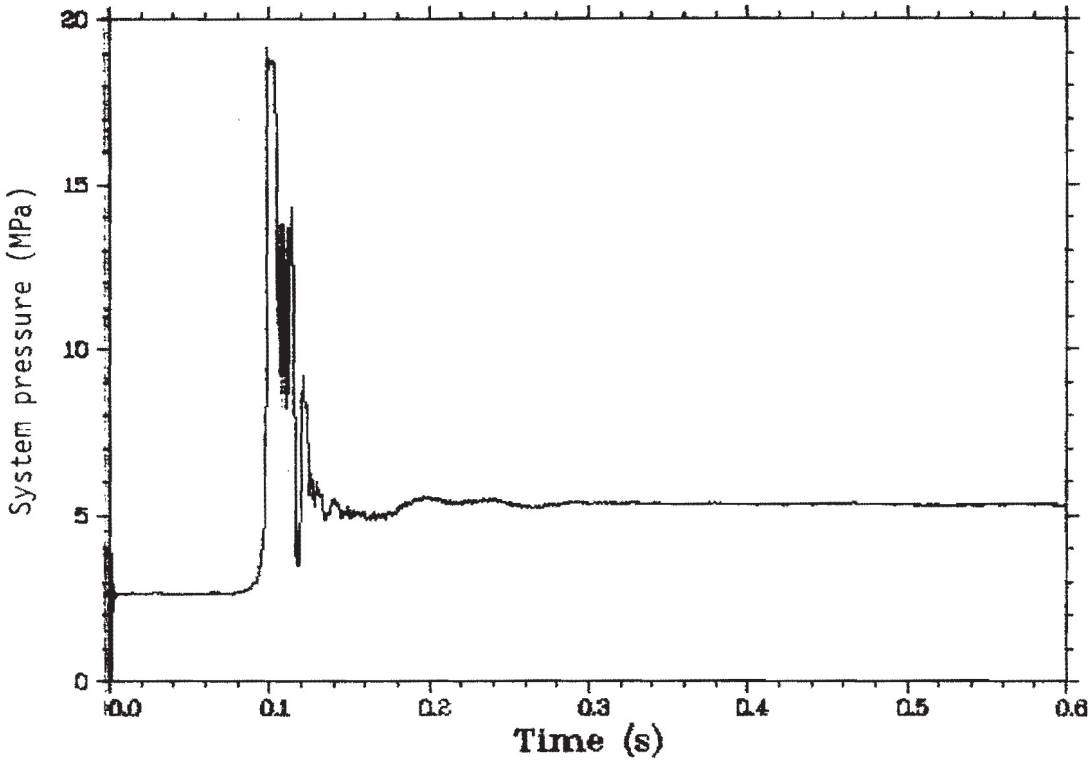

Fig. 12 Response of the 17 MPa Bell & Howell pressure transducer during the power burst of RIA-ST-4.

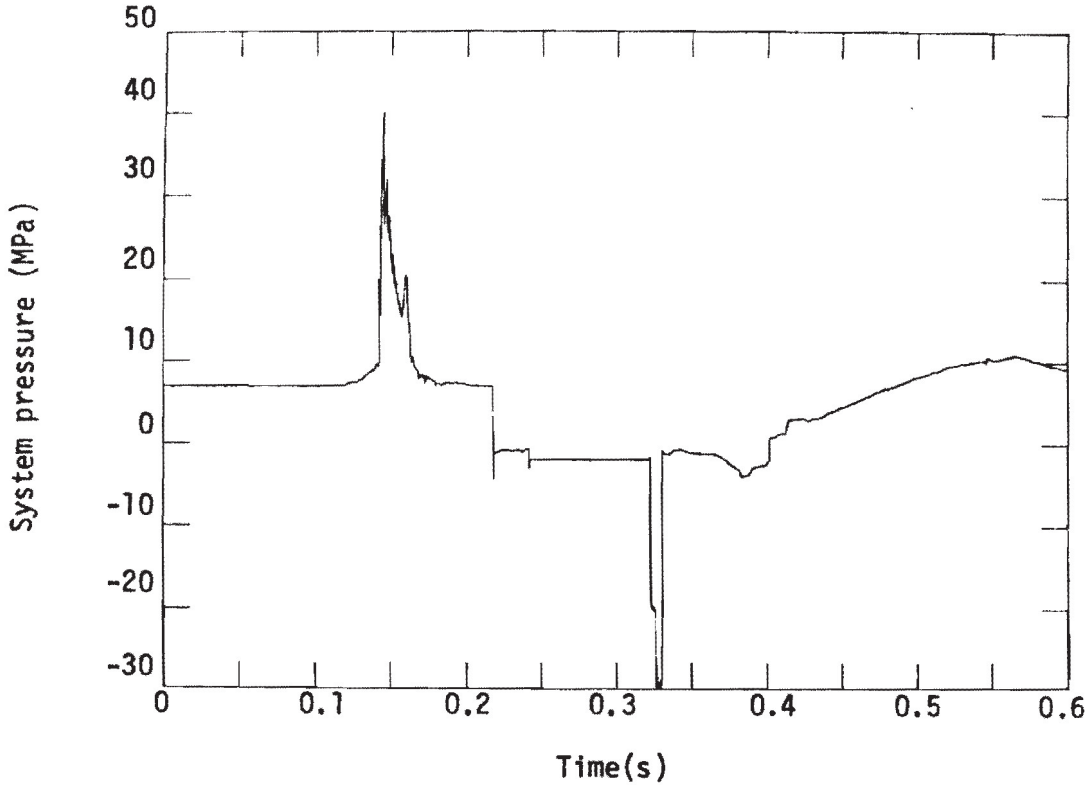

Fig. 13 Response of the lower 69 MPa EG&G pressure transducer during the power burst of RIA-ST-4.

saturated at about 19 MPa corresponding to a rise of about 16 MPa. The slope of the pressure rise was estimated to be approximately 20 MPa/ms.

The 69 MPa EG&G pressure transducer was connected via a small diameter tube into the inlet area of the flow shroud. The LVDT just above it was removed prior to RIA-ST-4, therefore this 69 MPa pressure transducer was directly in-line with the source pressure pulse. Figure 13 shows the output of the 69 MPa pressure transducer. The peak of the curve represents a pressure rise of 28.2 MPa with a rise time of 1.6 ms. The experiment predictions report for the Scoping Test indicated that a 475 cal/g energy deposition would result in a pressure pulse of 24.1 MPa with pressure doubling of 31.7 MPa at 7 ms after fuel dispersal.

Table VIII summarizes the pertinent data obtained from each of these transducers for RIA-ST-4. There were no significant pulses detected in the loop piping.

4.4 Instrument Sensitivity

The final objective of the RIA Scoping Test was to determine the sensitivity of the test instrumentation to high transient radiation exposures. This determination was essential for proper data evaluation in the RIA Series 1 tests. To facilitate the instrumentation evaluation, several environmentally isolated devices were added to the test train. The instruments intended specifically for instrument sensitivity evaluation during the RIA Scoping Test were as follows:

(1) One 17 MPa Kaman, one 17 MPa EG&G, and one 69 MPa EG&G pressure transducer. The Kaman was located in the flow bypass region near the top of the test rod, while the EG&G transducers were fixed to the hanger rod in the IPT upper plenum. All three pressure transducers were sealed to eliminate response due to coolant pressure changes.

TABLE VIII

PRESSURE DATA FROM RIA-ST-4 POWER BURST

Pressure Transducer	Location	Pressure Increase	Total Peak Pressure	Rise[a] Time
17 MPa EG&G	Flow bypass near top of rod.	1.8 MPa (250 psi)	8.5 MPa (1240 psi)	4 ms
69 MPa EG&G	Upper plenum beyond particle screen.	2.1 MPa (310 psi)	8.9 MPa (1280 psi)	3 ms
69 MPa EG&G	Shroud inlet	28.2 MPa (4100 psi)	35.0 MPa (5080 psi)	1.6 ms
17 MPa B&H[b]	Source Region	15.9 MPa (2310 psi)	22.7 MPa (3290 psi)	20 MPa/ms (2900 psi/ms)

[a] Rise time is defined as the time from 10% to 90% of the pressure rise.

[b] Transducer saturated at a ΔP of 15.9 MPa (2310 psi). Rise time could not be obtained but slope was approximately 20 MPa/ms (2900 psi/ms).

(2) One 17 MPa Bell & Howell and one 17 MPa Schaevitz pressure transducer. The Bell & Howell transducer was connected via a tube to the source pressure region during RIA-ST-4. Both devices were fixed to the hanger rod. The 17 MPa Schaevitz was inoperable.

(3) One Linear Variable Differential Transformer (LVDT) with the core locked in position. This LVDT was located in the flow bypass region at approximately the same elevation as the active LVDT.

(4) One Type S thermocouple, located on the flow shroud at about the axial power peak elevation. This thermocouple was connected to the shroud for RIA-ST-1 only.

(5) Two strain gages, located on the flow shroud for radiation sensitivity evaluation. These were attached to the RIA-ST-1 flow shroud near the axial peak elevation.

Figure 14 illustrates the behavior of the blocked 69 MPa EG&G transducer. The device exhibited this behavior prior to and following each power burst of the Scoping Test with no visible change. It appears that the pressure transducer was defective. Figure 15 indicates the power burst behavior of the blocked 17 MPa Kaman and EG&G pressure transducers for the second burst of RIA-ST-1. This behavior was typical for all the bursts, varying in magnitude with the magnitude of the bursts. There was no significant difference in the indicated behavior with the occurence of fuel rod failure. Although the position of the Kaman transducer in the IPT subjected it to a higher neutron and gamma radiation than that experienced by the 17 MPa EG&G transducer, the pressure reponse of the Kaman showed less disturbance in all cases.

The Schaevitz pressure transducer was added to the test train because the LVDT-type device had not been previously used in PBF. For RIA-ST-1, the pressure transducer was connected via a small diameter

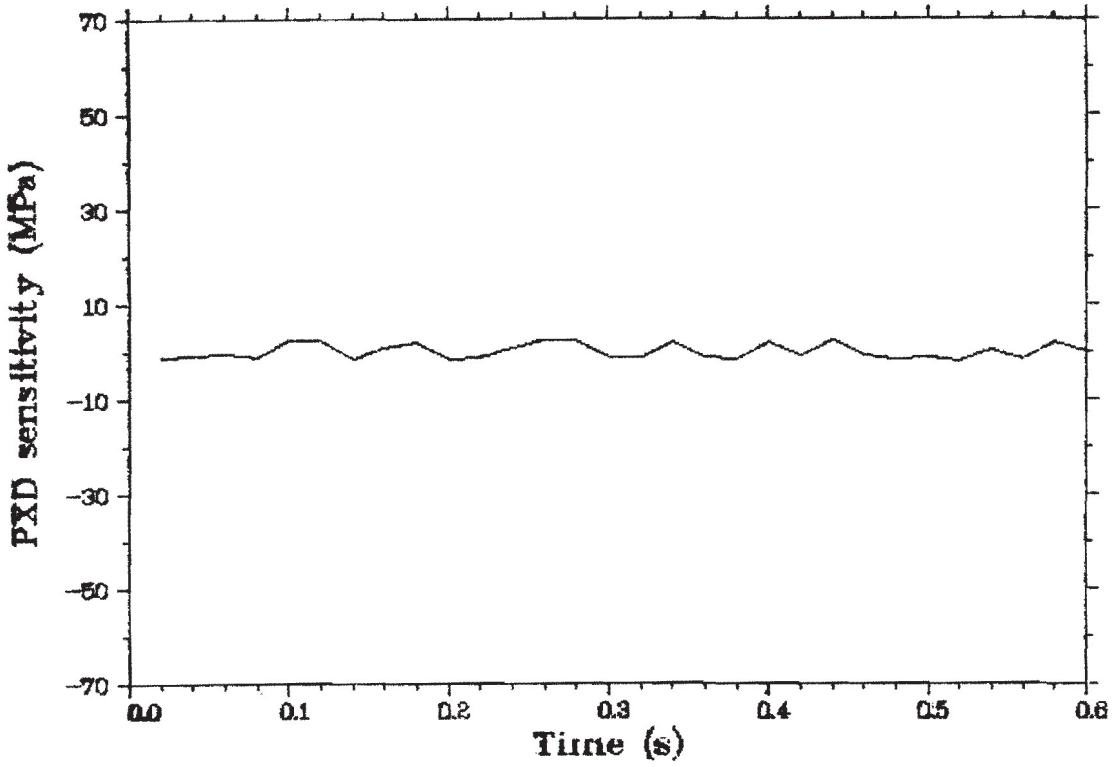

Fig. 14 Radiation sensitivity of the 69 MPa EG&G pressure transducer. (RIA-ST-4)

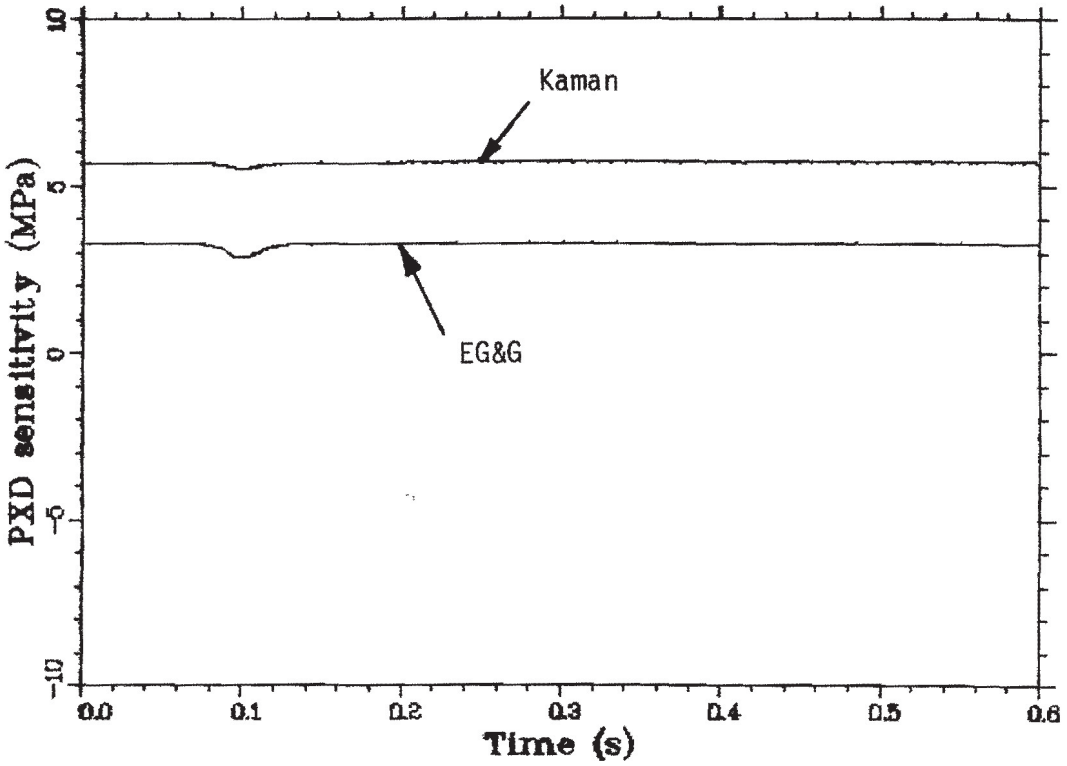

Fig. 15 Radiation sensitivity of the 17 MPa EG&G and Kaman pressure transducers. (RIA-ST-1, Burst 2)

tube to the source pressure region inside the flow shroud. A damaged transducer lead resulted in water intrusion which rendered the device useless, therefore, no data was obtained to evaluate this device.

The 17 MPa Bell & Howell pressure transducer provided the pressure response indicated in Figure 16 to the power burst and subsequent rod failure of RIA-ST-1. There is no radiation sensitivity indicated. The transducer was connected via a small diameter tube to the source pressure region inside the flow shroud for RIA-ST-4. The pressure response for that phase was illustrated by Figure 12 in Section 4.3.

Figure 17 shows the response of the locked LVDT to the large power burst of RIA-ST-4. The trace shows no indication of radiation sensitivity. That was typical during all the power bursts.

During RIA-ST-1, a Type S thermocouple and two strain gages were fixed to the outside of the flow shroud near the axial peak elevation. Figure 18 shows the response of the thermocouple to the power burst and subsequent rod failure. This trace is nearly identical to that for the first burst of RIA-ST-1 where there was no fuel rod failure. It can be presumed, therefore, that the slight increase in temperature indicated at 24 s on the curve is a result of radiation sensitivity (gamma heating) of the thermocouple. There was a more significant effect to the strain gages. Figure 19 illustrates the strain gage response to the second power burst of RIA-ST-1. Fuel rod failure does not contribute to this response as the strain gage trace for the first burst of RIA-ST-1 is similar, differing only in magnitude. The magnitude of strain gage response corresponds to the radiation intensity of each burst. In this case a 70% offset is induced which appears to be permanent.

Although a control device was not included in the Scoping Test, a significant problem was observed with the power burst response of the turbine flowmeters. Figure 20 illustrates the flowmeter response for RIA-ST-4. The rod failure during the RIA-ST-4 power burst occurred

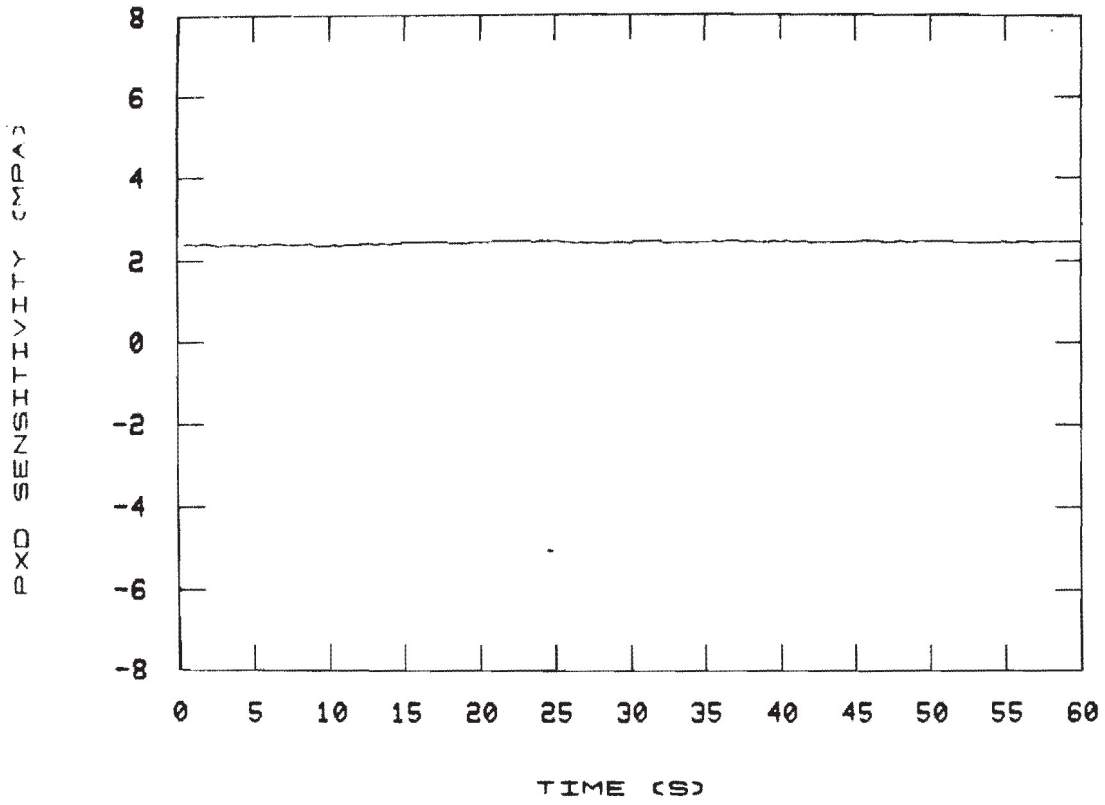

Fig. 16 Radiation sensitivity of the 17 MPa Bell & Howell pressure transducer. (RIA-ST-1, Burst 2)

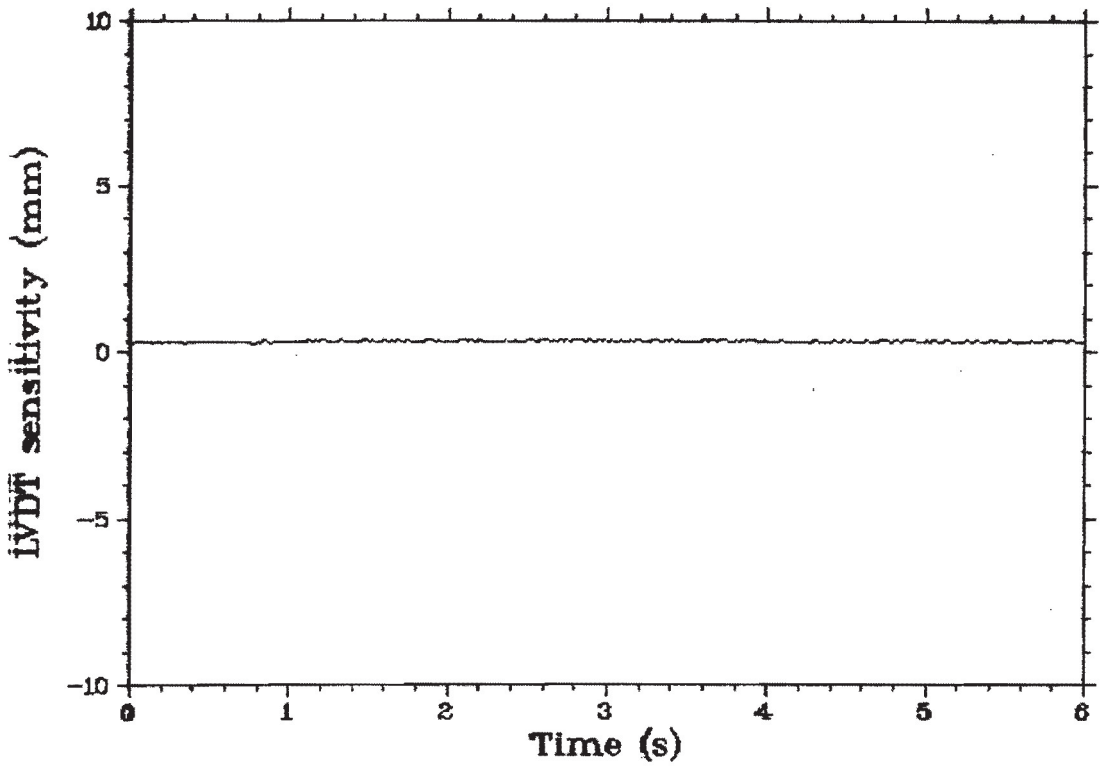

Fig. 17 Radiation sensitivity of the linear variable differential transformer. (RIA-ST-4)

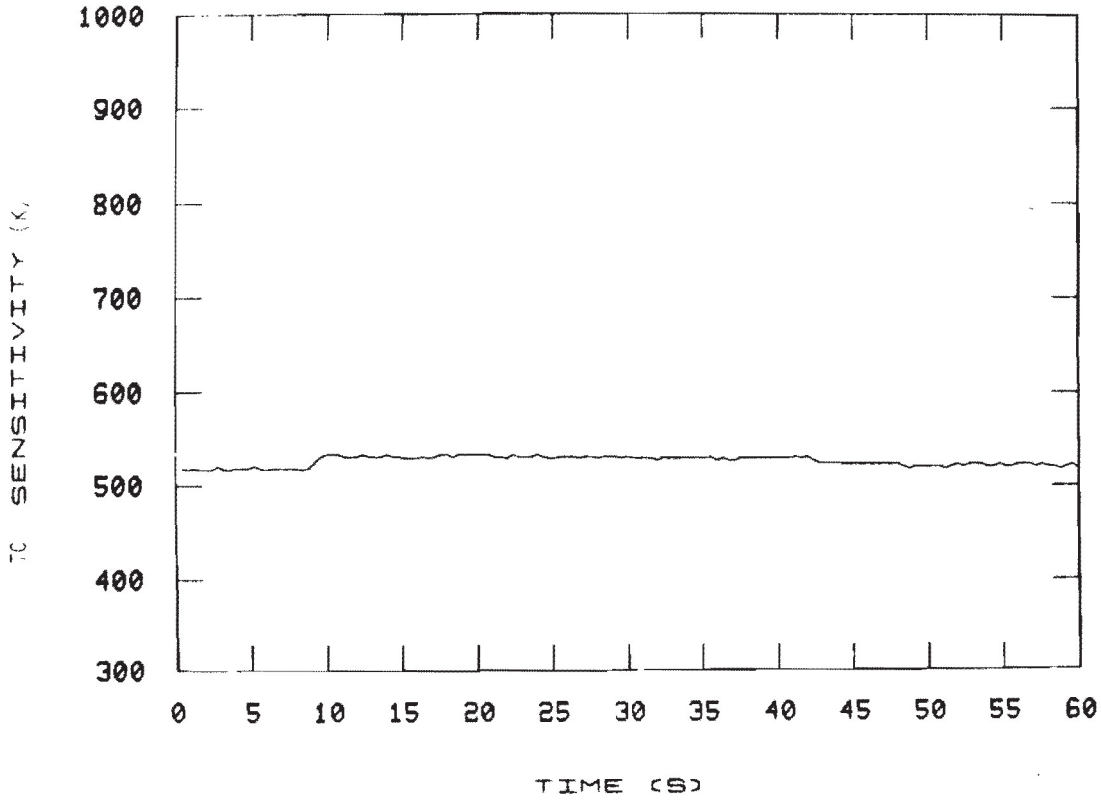

Fig. 18 Radiation sensitivity of the Type S thermocouple. (RIA-ST-1, Burst 2)

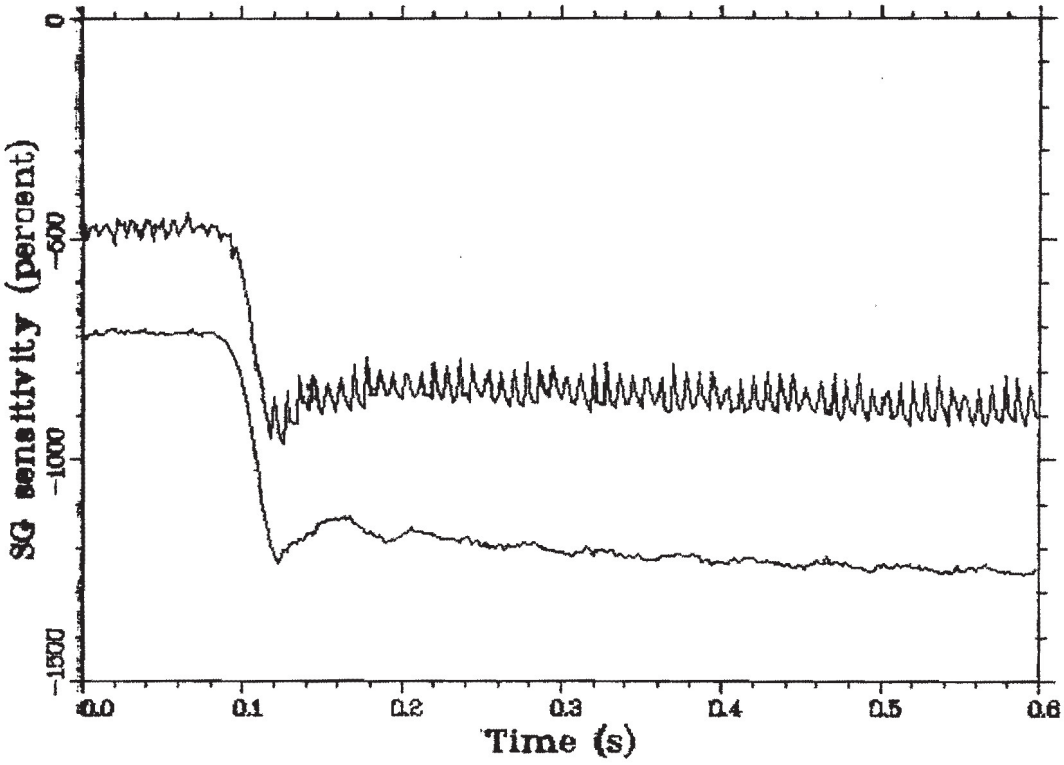

Fig. 19 Radiation sensitivity of the strain gages. (PIA-ST-1, Burst 2)

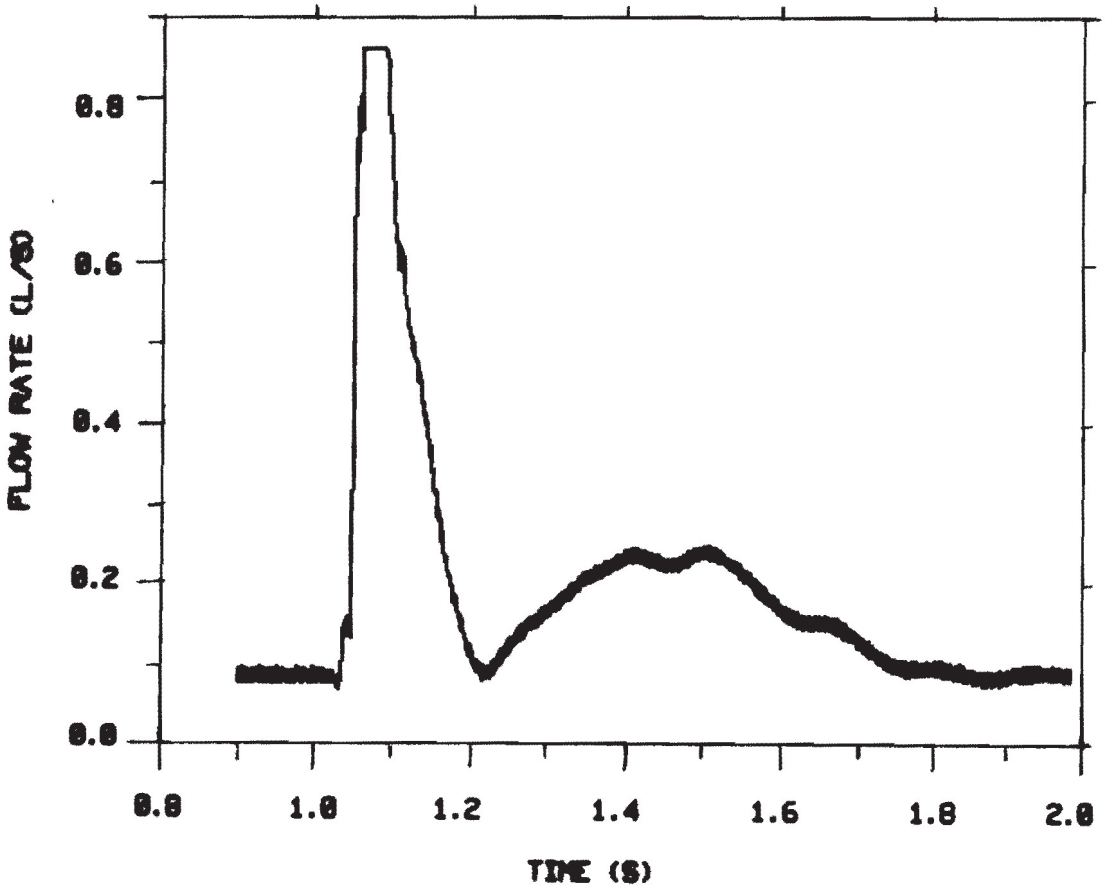

Fig. 20 Flowmeter response during the power burst and rod failure of RIA-ST-4.

about 4 ms after the time of peak power. The failure was severe and caused significant coolant vaporization, subsequent flow shroud voiding, and probably flow reversal of the flow shroud inlet. The flowmeters are not bi-directional and will indicate positive flow even though it is negative, however, the flowmeter response should pass through zero anytime the flow changes direction. The flowmeter behavior indicated by Figure 20 is not as expected. There is no drop in flow following the rod failure. Instead, the indication is of a sharp increase in flow until the signal conditioning is saturated at 880 cm^3/s, followed by a decrease.

The pickup coils to a turbine flowmeter generate a sinusoidal current corresponding to the rotation of the turbine. This sinusoidal wave is converted to a flowrate indication by electronically counting the peaks on the wave. It is believed that the power burst adds a high frequency noise to the sinusoidal wave signal, thus causing the electronic counter to see many more peaks than can be attributed to the flow turbine rotation. This artificially high number of peaks translates to a much higher flow indication than there should be.

5. POSTTEST PHOTOGRAPHS

Figures 21 through 26 illustrate the posttest condition of the rods from RIA-ST-2 and RIA-ST-3. The appearance of the rod from RIA-ST-1 was similar to that of the RIA-ST-2 rod.

Figure 21 shows the remnants of the fuel stack of the RIA-ST-2 rod between the 0.370 and 0.470 m rod elevations. Most of the fuel was gone, and only a small portion of the original fuel inventory in this region remained within the flow shroud. Preliminary examination indicates that the fuel in this region did not melt. A longitudinal slit in the cladding of this rod was observed between the 0.520 and 0.600 m rod elevations in the 0^{o}-180^{o} plane. A large percentage of the fuel was missing, as is shown in Figure 22. The cladding in this region is extremely brittle and may have experienced melting. Bulging of the cladding at the pellet interface (bambooing) was observed between the 0.675 and 0.780 rod elevations of the rod from RIA-ST-2 and is shown in Figure 23. Small, circumferentially oriented cracks occurred within the bulge.

The flux peak region of the rod from RIA-ST-3 (0.36 to 0.450 m) is shown in Figure 24. Severe oxidation and cladding deformation are evident. No breaks in the cladding were detected. Cladding waisting near the 0.60 m elevation of this rod is seen in Figure 25. The cladding in this portion of the rod has collapsed into pellet interfaces and pellet defects (0.645 m). Only two interfaces of the RIA-ST-3 rod exhibited bambooing. These occurred near 0.66 m, and are shown in Figure 26.

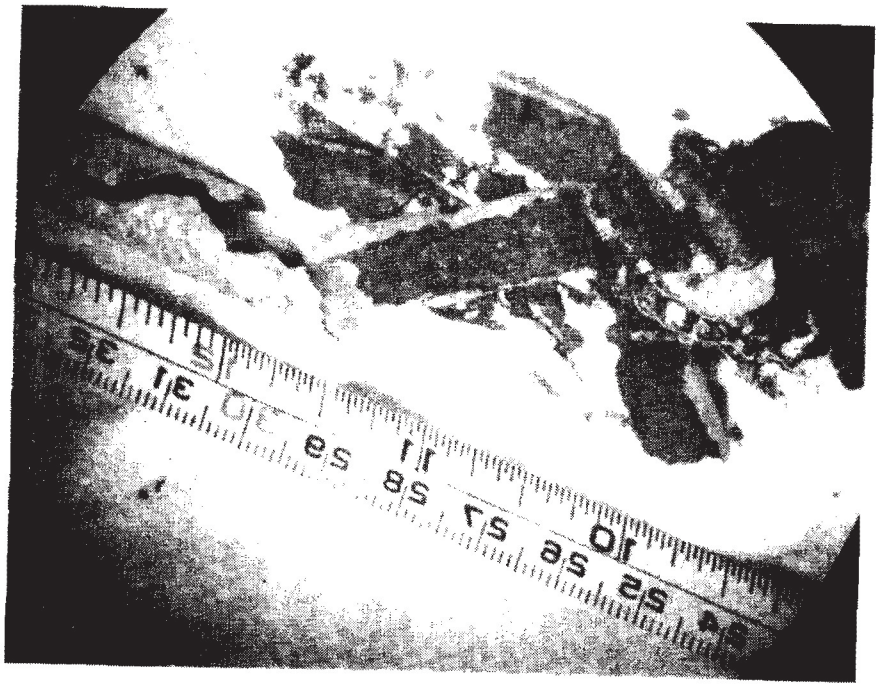

Fig. 21 Posttest photograph of fuel rod from RIA-ST-2 between 0.370 and 0.470 m rod elevations

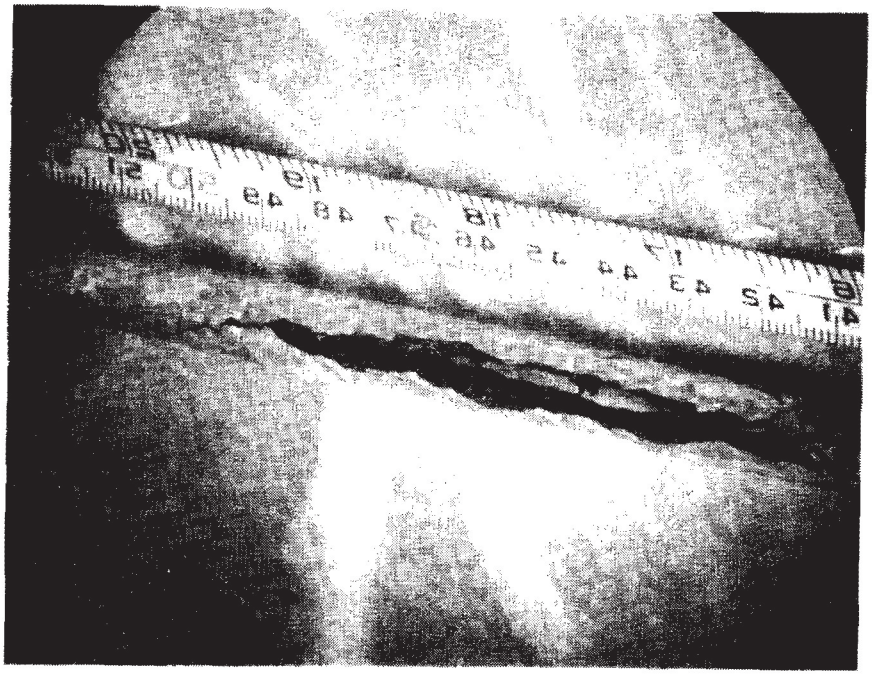

Fig. 22 Posttest photograph of fuel rod from RIA-ST-2 between the 0.520 and 0.600 m rod elevations

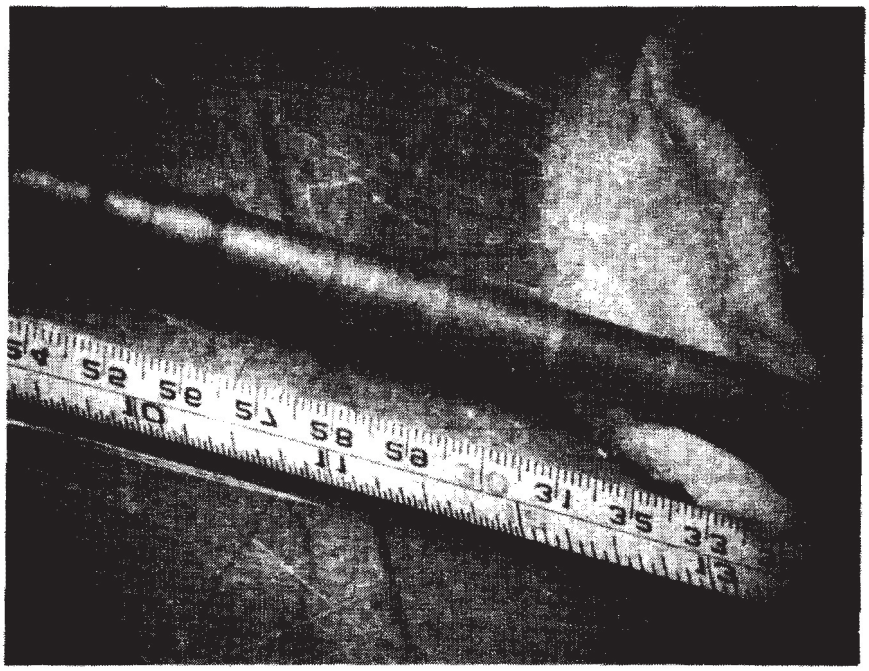

Fig. 23 Posttest photograph of fuel rod from RIA-ST-2 between the 0.675 and 0.780 m rod elevations

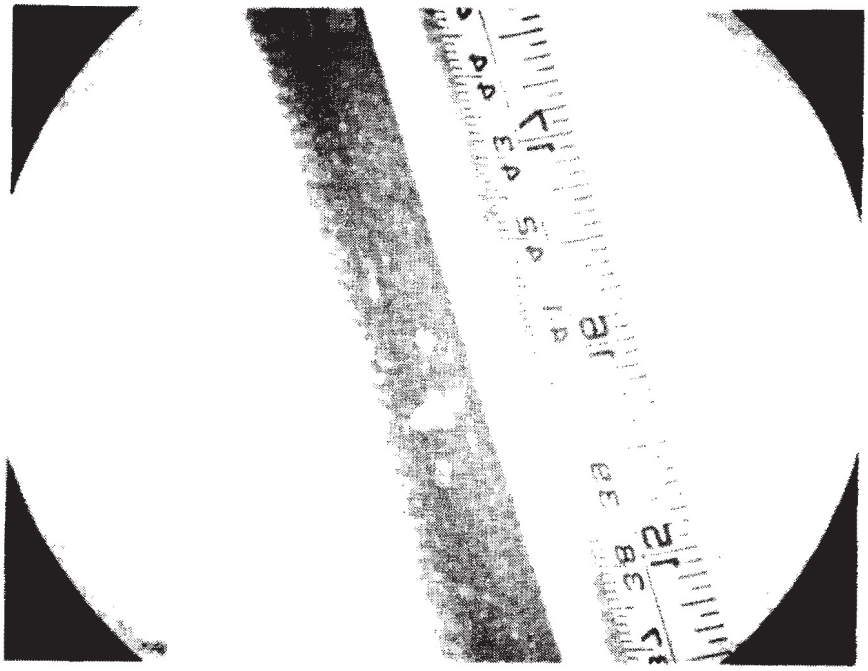

Fig. 24 Posttest photograph of fuel rod from RIA-ST-3 between the 0.360 and 0.450 m rod elevations

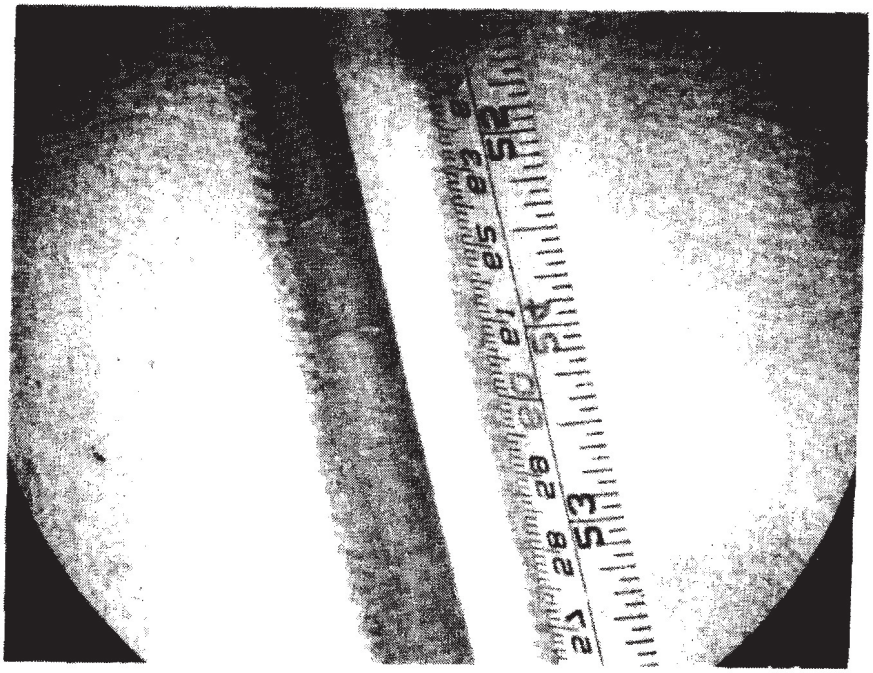

Fig. 25 Posttest photograph of fuel rod from RIA-ST-3 near 0.600 m rod elevation

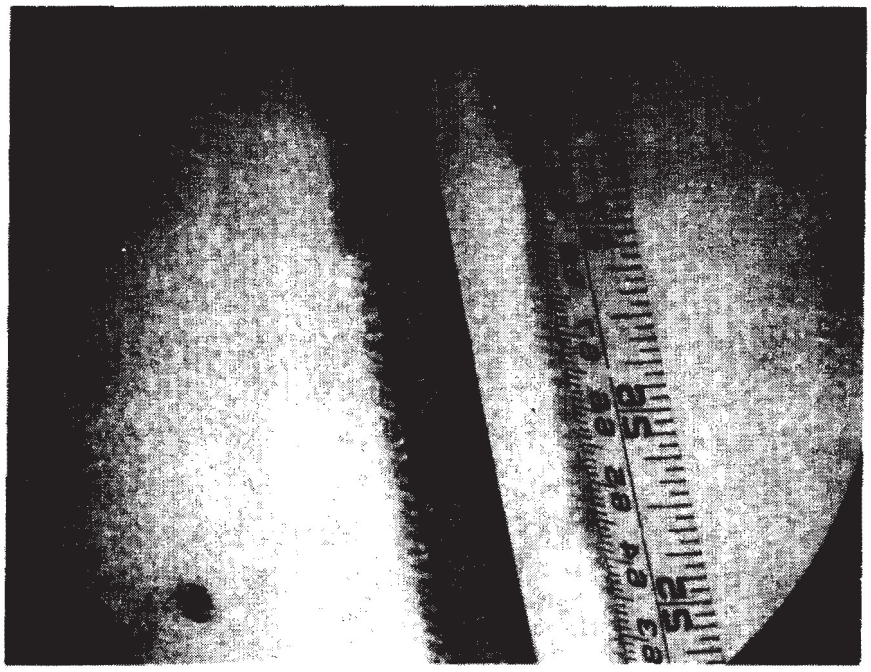

Fig. 26 Posttest photograph of fuel rod from RIA-ST-3 near 0.660 m rod elevation

6. FISSION PRODUCT DETECTOR

The fission product detection system was operated during all RIA-ST power bursts to establish rod failure. The gross gamma and delayed neutron activity provided a relative indication of the failure extent during the tests; the gamma spectroscopic system data will provide the concentration of individual isotopes released during and following the rod failure.

Following the second power burst of RIA-ST-1, and the power bursts of RIA-ST-2 and RIA-ST-4, rod failure was indicated by an increased gamma count rate as shown in Figures 27, 28, and 30, respectively. During RIA-ST-3 an increase was not observed indicating failure had not occurred (Figure 29). There was a significant difference in the maximum count rates measured during RIA-ST-1, RIA-ST-2, and RIA-ST-4 indicating that the RIA-ST-4 rod sustained more extensive failure.

The delay time from the burst to the increase in gamma activity at the detector station during RIA-ST-1 and RIA-ST-2 was approximately 7.5 minutes; during RIA-ST-4 the delay time was $\sim$3.25 minutes. The difference in delay time is not due to differences in loop flow rates since the loop flow rate was nearly the same for each power burst.

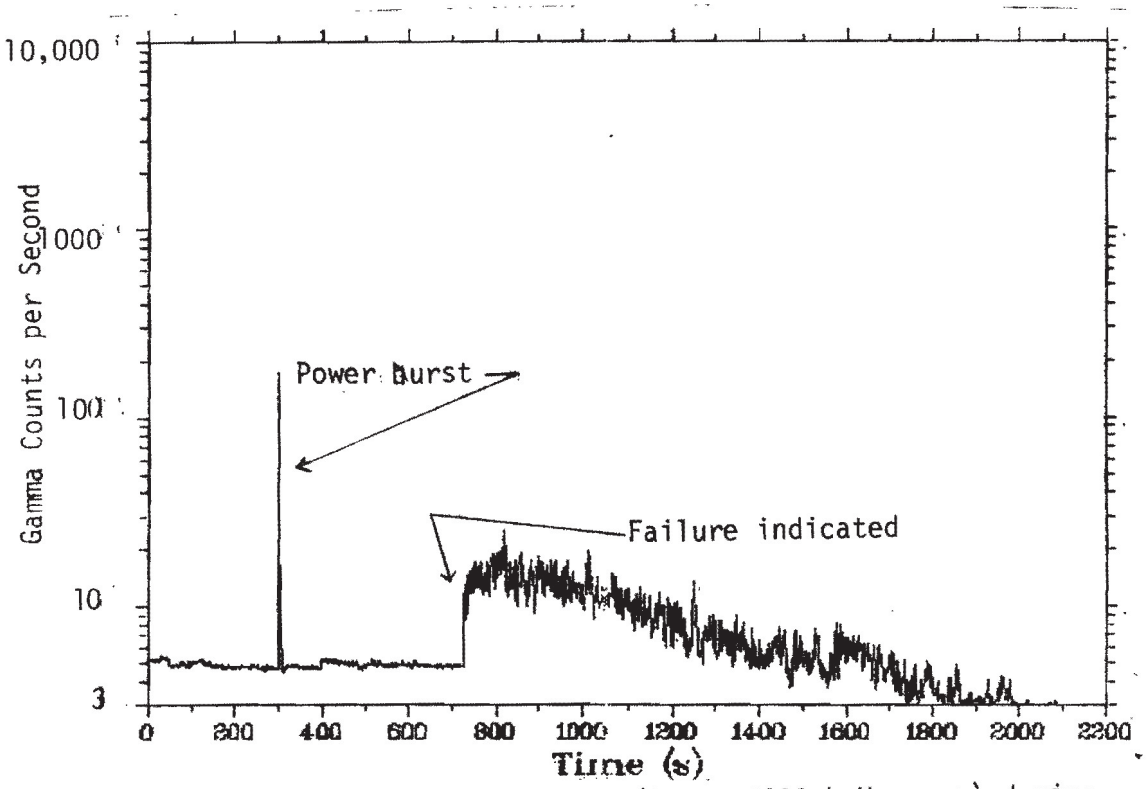

Fig. 27 Gross gamma count rate (150 - 3400 keV range) during Scoping Test 1 burst 2.

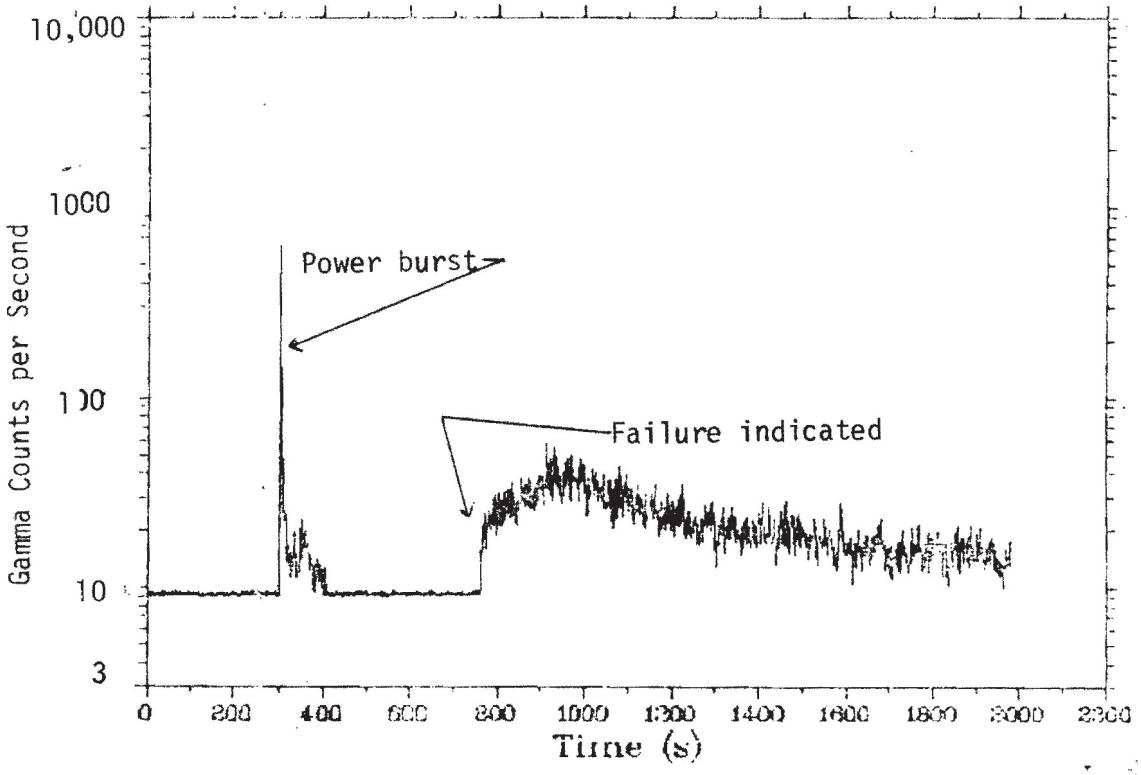

Fig. 28 Gross gamma count rate (150 - 3400 keV range) during Scoping Test 2.

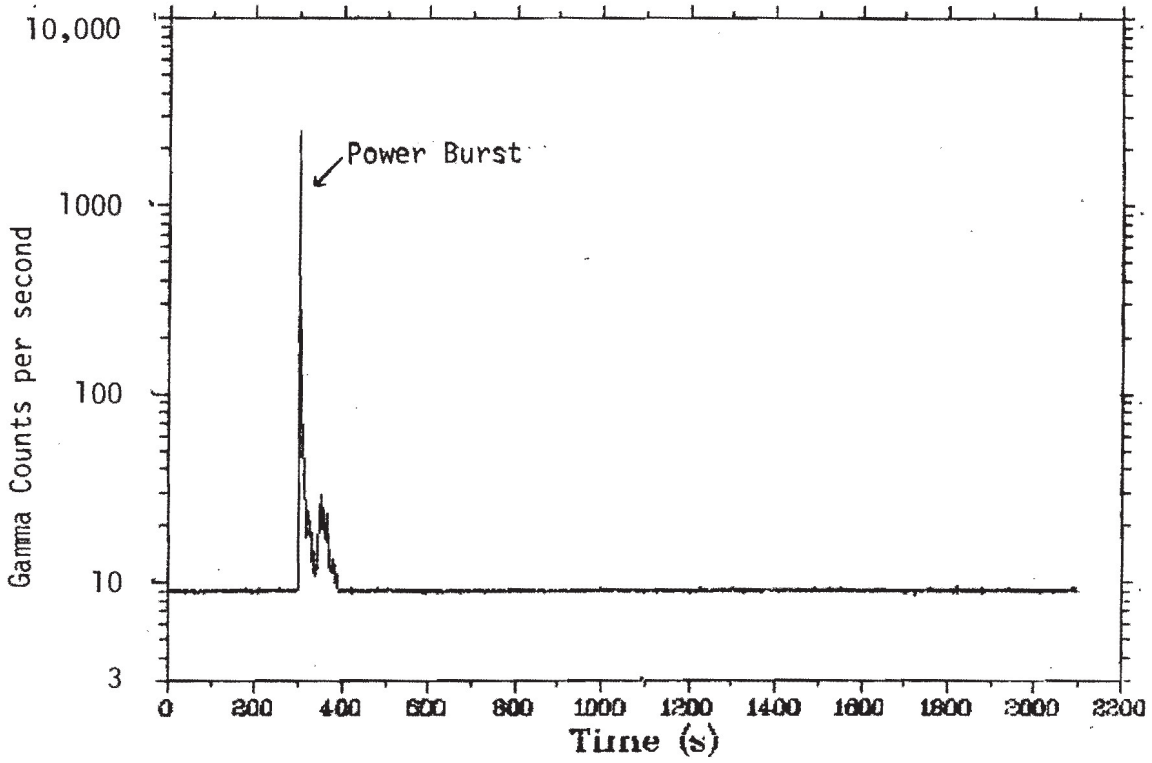

Fig. 29 Gross gamma count rate (150 - 3400 keV range) during Scoping Test 3. No failure indicated.

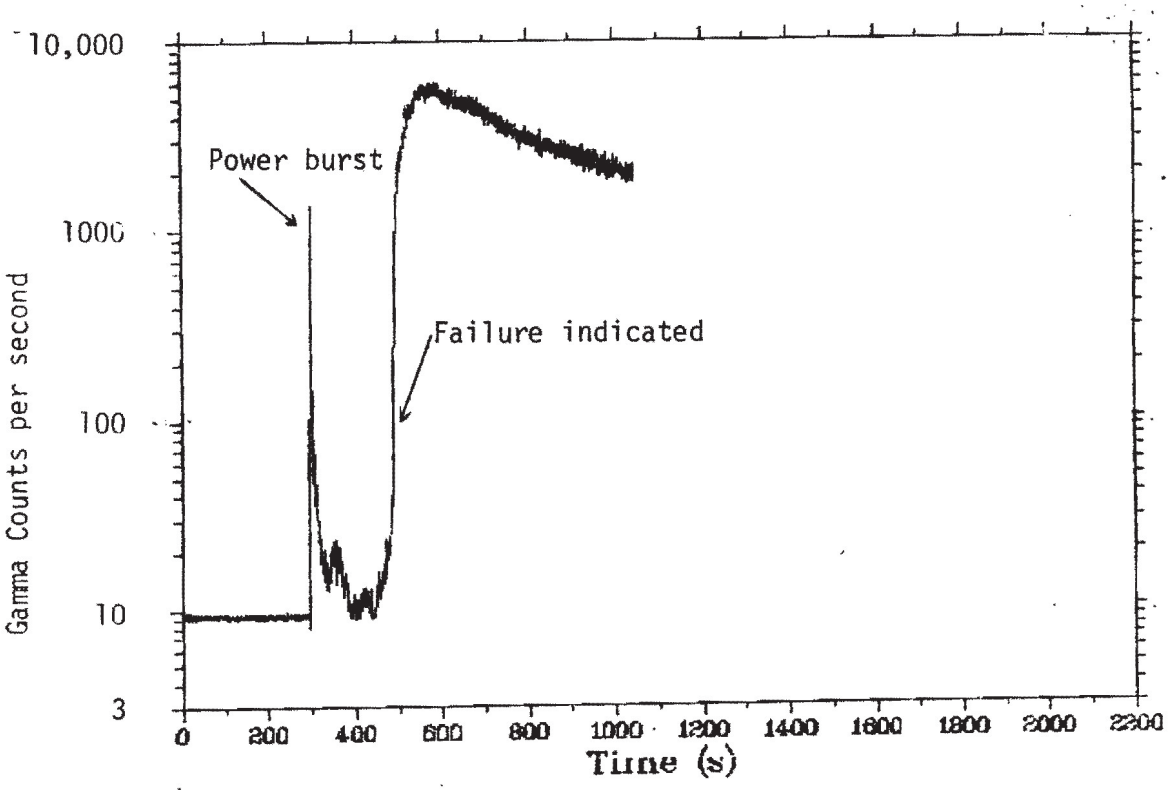

Fig. 30 Gross gamma count rate (150 - 3400 keV range) during Scoping Test 4 power burst.

CONCLUSIONS

The RIA Scoping Test has provided data regarding the four main objectives of the test. These results are summarized below.

(1) Definite conclusions regarding the applicability of calorimetric measurements to determine fuel rod energy during a power burst must await radiochemical analysis results. The calculated power calibration ratio of fuel rod power to reactor power was in excellent agreement with reactor physics calculations. Relating the calorimetric power calibration results to the SPNDs yielded fuel rod energy depositions about 25% higher than those determined from the core power chambers. Current evidence indicates that the SPND values are in error. Further analysis will be required.

(2) The failure threshold of unirradiated fuel rods determined calorimetrically under BWR hot startup conditions is between 218 and 256 cal/g UO_2 (pellet surface energy at the axial flux peak). These values are slightly below those of pretest predictions.

(3) Although a large source pressure was measured during RIA-ST-4, only low magnitude pressures were measured elsewhere in the IPT and loop piping.

(4) The most significant problem regarding instrument performance is the turbine flowmeter. Resolution of this problem is required before meaningful coolant flow time history measurements during a power burst can be made for future RIA tests. Another RIA test concern is the short operating lifetime due to bearing seizure of the turbine flowmeters following fuel rod failure. None of the turbine flowmeters would rotate following RIA-ST-1, RIA-ST-2, or RIA-ST-4.

In addition, new information regarding consequences of fuel rod failure under BWR hot startup conditions has been provided. The RIA Scoping Test has shown that large amounts of UO_2 can be expected to be expelled or washed out into the coolant for an RIA event occurring at high temperature, pressure, and forced coolant flow conditions. Only a slight loss of fuel from the cladding occurred during previous tests conducted at CDC and NSRR in a closed capsule at ambient conditions.

8. REFERENCES

1. R. S. Semken, T. Inabe, Z. R. Martinson, Reactivity Initiated Accident Test Series RIA Scoping Test Experiment Operating Specification, TFBP-TR-217 (May 1978).

2. R. S. Semken, A. M. Eaton, R. H. Smith, S. C. Resch, Reactivity Initiated Accident Test Series RIA Scoping Test Experiment Predictions, TFBP-TR-275 (June 1978).

QLR

CONTROLLED DISTRIBUTION

R. G. Ambrosek
R. W. Barber (DOE) (2)
R. L. Benedetti
M. P. Bohn
R. J. Buckland
D. Coleman
J. G. Crocker
B. R. DaBell
J. A. Dearien, Jr.
G. H. Dechman
W. F. Domenico
C. O. Doucette
R. J. Drake
E. E. Felix
S. R. Gossmann
W. R. George
R. N. Hagen
J. C. Haire
D. E. Hill
A. M. Jensen
W. V. Johnston (NRC) (2)
J. E. Koch
M. M. Larson
B. H. Little (DOE)
W. G. Lussie
Z. R. Martinson (10)
R. W. Marshall, Jr.
R. D. McCormick
F. A. Meichle
E. V. Mobley
M. N. Monson
P. North
S. Resch
L. J. Siefken
J. Sielinsky
D. L. Smith
L. A. Stephan
F. E. Stoll
P. O. Strom (NRC)
K. G. Therp
R. E. Tiller (DOE) (4)
E. L. Tolman
R. D. Ulrich
R. VanHouten (NRC)
C. E. White
L. J. Ybarrondo
M. W. Young
T. E. Young
J. O. Zane
H. J. Zeile
C. L. Zimmermann
R. L. Ooley
R. L. Persons
All Division Personnel